
A LONG-SHORT FLOW-MAP PERSPECTIVE FOR DRIFTING MODELS

Zhiqi Li

School of Interactive Computing
Georgia Institute of Technology
zli3167@gatech.edu

Bo Zhu

School of Interactive Computing
Georgia Institute of Technology
bo.zhu@gatech.edu

ABSTRACT

This paper provides a reinterpretation of the Drifting Model Deng et al. [2026] through a semigroup-consistent long-short flow-map factorization. We show that a global transport process can be decomposed into a long-horizon flow map followed by a short-time terminal flow map admitting a closed-form optimal velocity representation, and that taking the terminal interval length to zero recovers exactly the drifting field together with a conservative impulse term required for flow-map consistency. Based on this perspective, we propose a new likelihood learning formulation that aligns the long-short flow-map decomposition with density evolution under transport. We validate the framework through both theoretical analysis and empirical evaluations on benchmark tests, and further provide a theoretical interpretation of the feature-space optimization while highlighting several open problems for future study.

Keywords One-Step Generation, Flow Map Method, Drifting Model, Closed-Form Solution

1 Introduction

Flow-based generative modeling formulations such as Flow Matching Lipman et al. [2023, 2024] describe the evolution of a probability distribution through a time-dependent velocity field that transports a simple base distribution to the data distribution. While these continuous-time methods provide stable regression objectives and strong empirical performance, sample generation typically requires numerically integrating the learned dynamics over tens to hundreds of steps. This sampling cost has motivated the development of few-step and one-step generative frameworks Frans et al. [2025], Geng et al. [2025a,b], Song et al. [2023], Zhou et al. [2025], which aim to learn direct transport maps that produce samples in a single evaluation.

Among these approaches, the Drifting Model Deng et al. [2026] was proposed as a deterministic one-step generator motivated from a distribution-matching perspective and has demonstrated competitive results. The method learns a deterministic mapping f such that the pushforward of the noise distribution by f matches the data distribution, enabling one-step sampling by $x_1 = f(x_0)$. While the method is well justified from its original formulation, its connection to established transport and flow-map frameworks has not yet been explicitly characterized. In particular, it is of interest to understand how a one-step transport map relates to trajectory-consistent flow-map structures, and how dataset-level supervision arises within such a formulation without multi-step distillation or optimization.

In this paper, we provide a flow-map-based interpretation and derivation of the Drifting Model. Our key message is that the Drifting Model can be derived from a semigroup-consistent long-short flow-map decomposition coupled with a terminal closed-form optimal velocity. Specifically, we factorize the global transport map according to the semigroup property of flow maps into a long-range, initial flow map and a short-range, terminal flow map, $\psi_{0 \rightarrow 1} = \psi_{1-\Delta t \rightarrow 1} \circ \psi_{0 \rightarrow 1-\Delta t}$, where the terminal flow map is evaluated using the closed-form optimal velocity Bertrand et al. [2025] near the final time. This construction yields direct dataset-level supervision for the terminal correction while preserving trajectory consistency for the remaining component. By analyzing the limit as $\Delta t \rightarrow 0$, we show that the resulting infinitesimal terminal map recovers exactly the drifting formulation, with the attraction term arising from the first-order expansion of the closed-form velocity and the impulse term appearing in the second-order expansion as a conservative correction required for flow-map consistency.

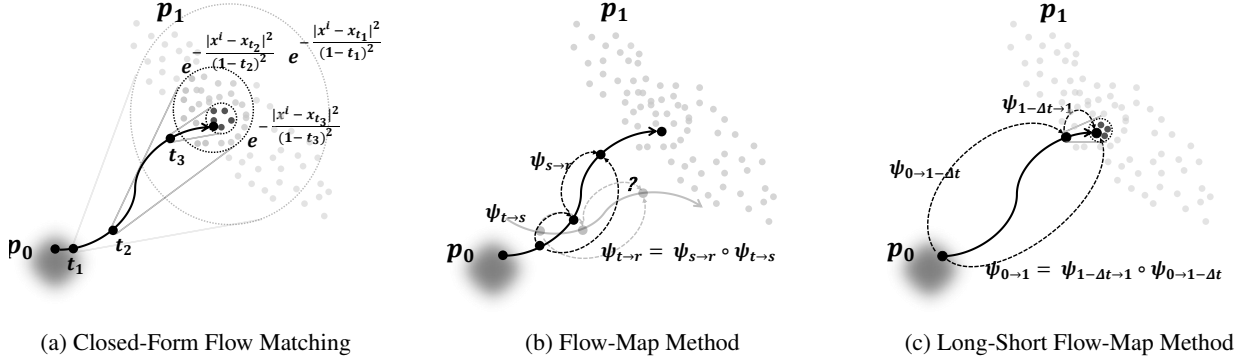


Figure 1: (a) Closed-form Flow Matching (subsection 2.1) requires kernel-weighted aggregation over data points, which becomes prohibitively expensive when the kernel is diffuse (far from $t = 1$). (b) Flow-map training (subsection 2.2) enforces trajectory consistency but is difficult to supervise directly from data, so spurious consistent paths (e.g., the semi-transparent segment) can still satisfy the constraint. (c) Our Long-Short Flow Map method (section 3) applies a closed form estimator on the short step $\psi_{1-\Delta t \rightarrow 1}$ as $\Delta t \rightarrow 0$ (subsection 3.1 first order, subsection 3.2 second order), which provides dataset grounded supervision for learning the long step $\psi_{0 \rightarrow 1-\Delta t}$ and thereby addresses the challenges of both closed form Flow Matching and flow map methods.

This long-short flow-map perspective offers a structured way to understand the Drifting Model and helps interpret several of its design choices, including the simultaneous presence of attraction and impulse components and the emergence of multiple feature representations. Building on this viewpoint, we further introduce a likelihood-learning formulation aligned with the induced density evolution under transport and propose a squared-kernel modification to improve theoretical consistency with the noise’s form. We validate the resulting framework on both illustrative and benchmark tests and conclude with open questions in feature-space optimization.

2 Background

2.1 Closed-Form Flow Matching

Given a dataset $\mathcal{D} = \{x^i \in \mathcal{X}\}_{i=1}^n$ drawn from an unknown data distribution p_{data} on space $\mathcal{X} \subset \mathbb{R}^d$, Flow Matching aims to learn a continuous-time velocity field $u(x, t)$, $t \in [0, 1]$, that transports a base distribution p_0 , typically a Gaussian distribution $\mathcal{N}(0, \sigma^2)$, to the target distribution $p_1 = p_{\text{data}}$ along a continuous path of intermediate distributions $(p_t)_{t \in [0,1]}$. Once $u(x, t)$ is learned, samples from p_1 can be generated by integrating the ordinary differential equation

$$\frac{dx_t}{dt} = u(x_t, t), \quad x_0 \sim p_0. \quad (1)$$

The family of distributions $(p_t)_{t \in [0,1]}$ is induced by the velocity field $u(x, t)$, and their relationship is governed by the continuity equation

$$\frac{\partial}{\partial t} p_t(x) + \nabla \cdot (p_t(x) u_t(x)) = 0 \quad (2)$$

A natural training objective for training $u_t^\theta(x)$ is $\mathcal{L}^{FM}(\theta) = \mathbb{E}_{t, x \sim p_t(x)} \|u_t^\theta(x) - u_t(x)\|^2$, which directly matches the model velocity to the reference velocity field. However, this objective cannot be optimized in practice, since both $u_t(x)$ and the marginal distribution $p_t(x)$ are hard to be calculated directly from the dataset. To incorporate supervision from data, Flow Matching introduces conditional velocities $u_t(x|x_1) = \frac{x_1 - x}{1-t}$ and conditional flows $\psi_t(x|x_1) = t(x_1 - x) + x$ for arbitrary $x_1 \in \mathcal{X}$. These conditional quantities induce a conditional distribution $p_{t|1}(\cdot|x_1) = (\psi_t(\cdot|x_1))_\# p_0$, and the marginal velocity field and distribution can then be recovered by marginalization $u_t(x) = \mathbb{E}_{x_1 \sim p_{1|t}(x|x_1)} [u_t(x|x_1)]$ and $p_t(x) = \mathbb{E}_{x_1 \sim p_{1|t}(x|x_1)} [p_{t|1}(x|x_1)]$ respectively. Based on these constructions, Flow Matching defines the conditional surrogate objective

$$\mathcal{L}_c^{FM}(\theta) = \mathbb{E}_{t, x_1 \sim p_{\text{data}}, x \sim p_{t|1}(x|x_1)} \|u_t^\theta(x) - u_t(x|x_1)\|^2, \quad (3)$$

which admits supervision from data samples. It has been shown that $\nabla_\theta \mathcal{L}_c^{FM}(\theta) = \nabla_\theta \mathcal{L}^{FM}(\theta)$ and therefore \mathcal{L}_c^{FM} serves as a valid surrogate for optimizing \mathcal{L}^{FM} .

In Bertrand et al. [2025] and earlier work, the authors show that the Flow Matching objective in Equation 3 admits a closed-form optimal solution, which can be summarized as the following property.

Theorem 2.1 (Closed-Form Solution of Flow Matching Bertrand et al. [2025]). *Equation 3 admits an optimal solution*

$$u_t^*(x) = \mathbb{E}_{x_1 \sim p_{1|t}(x_1|x)}[u_t(x|x_1)] = \frac{\mathbb{E}_{x_1 \sim p_{1|t}(x_1|x)}[x_1] - x}{1-t}, \quad (4)$$

which further admits a closed-form expression (see subsection A.1 for proof.)

$$u_t^*(x) = \frac{\mathbb{E}_{x_1 \sim p_1} \left[\frac{x_1 - x}{1-t} k_t(x_1, x) \right]}{\mathbb{E}_{x_1 \sim p_1} [k_t(x_1, x)]}, \quad k_t(y, x) = e^{-\frac{\|ty-x\|^2}{2(1-t)^2}} \quad (5)$$

In practice, this result is mainly used for analysis rather than directly computing the Flow Matching solution. We argue that the main obstacle to using the closed form as a solver arises away from $t = 1$, leading to the following challenge.

Challenge 2.2 (Challenge for Closed-Form Computation). *Directly using the closed-form optimal velocity $u_t^*(x)$ is impractical for training and sampling due to time-dependent concentration of kernel k_t . When t is close to 1, the factor $(1-t)^{-2}$ in the exponent makes k_t sharply concentrated, so the expectation is dominated by samples x_1 near x and the computation is effectively local. In contrast, when t is far from 1, the kernel is less concentrated, and evaluating the closed form requires aggregating contributions from a large portion of the data distribution, which is computationally prohibitive. Consequently, the closed-form velocity is tractable only near $t = 1$ and impractical at earlier timesteps.*

2.2 One-Step Flow Map

Flow Matching suffers from slow generation because sampling with $u(x_t, t)$ amounts to numerically discretizing the evolution in Equation 1, which typically requires many steps. Recent one-step generation methods instead learn a flow map, namely a family of mappings $\psi_{t \rightarrow r} : \mathcal{X} \rightarrow \mathcal{X}$ such that $\psi_{0 \rightarrow t}(x_0) = x_t$ for any trajectory $\{x_t\}_{t=0}^1$ that solves the ODE initialized at x_0 , and $\psi_{t \rightarrow r} = \psi_{0 \rightarrow r} \circ \psi_{0 \rightarrow t}^{-1}$ for any $t, r \in [0, 1]$. The flow map satisfies

$$\frac{\partial}{\partial t} \psi_{0 \rightarrow t} = u_t \circ \psi_{0 \rightarrow t}, \quad \psi_{0 \rightarrow 0} = \text{Id}_{\mathcal{X}}. \quad (6)$$

The marginal path can be written as a pushforward $p_t = (\psi_{0 \rightarrow t})_{\#} p_0$. Once $\psi_{t \rightarrow r}$ is learned, flow-map methods enable one-step generation via $x_1 = \psi_{0 \rightarrow 1}(x_0)$, and also few-step generation, e.g., $x_{0.5} = \psi_{0 \rightarrow 0.5}(x_0)$ followed by $x_1 = \psi_{0.5 \rightarrow 1}(x_{0.5})$ for two steps.

Flow maps are characterized by a trajectory consistency property, also known as the semigroup property, which is the key requirement when learning $\psi_{t \rightarrow r}$.

Proposition 2.3 (Trajectory Consistency). *For any $0 \leq t \leq s \leq r \leq 1$, the flow map satisfies*

$$\psi_{t \rightarrow r} = \psi_{s \rightarrow r} \circ \psi_{t \rightarrow s}. \quad (7)$$

To enforce trajectory consistency in learning, one can impose the following trajectory-consistency loss

$$\mathcal{L}^{TC}(\theta) = \mathbb{E}_{t,s,r,x_t \sim p_{t|1}(x|x_1), x_1 \sim p_1} \left[\left\| \psi_{t \rightarrow r}^\theta(x_t) - \psi_{s \rightarrow r}^\theta(\psi_{t \rightarrow s}^\theta(x_t)) \right\|_2^2 \right], \quad (8)$$

A central difficulty of optimizing Equation 8 is the lack of supervision from the dataset. Unlike the velocity field $u_t(x)$ in Flow Matching, flow maps do not admit an easily computable "conditional flow map" from data pairs (see Theorem A.1), which prevents us from writing a simple conditional objective analogous to the standard conditional Flow Matching loss.

To mitigate this issue, prior work has explored two broad strategies. *Progressive extension* methods, exemplified by Shortcut Frans et al. [2025], SplitMeanFlow Guo et al. [2025], and Flow Map Matching Boffi et al. [2025], start from the instantaneous limit $\lim_{s \rightarrow t} \frac{\psi_{t \rightarrow s}(x) - x}{s-t} = u_t(x)$ and progressively extend short-horizon supervision to longer horizons using the semigroup constraint in Proposition 2.3. *Continuous-based methods* take the $s \rightarrow t$ limit of Proposition 2.3 and derive a continuous equation of the form $\partial_t \psi_{t \rightarrow r}(x) + (u_t \cdot \nabla) \psi_{t \rightarrow r}(x) = 0$, which brings the instantaneous velocity u_t into the learning of long-horizon maps $\psi_{t \rightarrow r}$; since u_t admits dataset supervision through its conditional form $u_t(x|x_1)$ in Flow Matching, this provides a way to inject data-driven supervision into flow-map learning, as exemplified by MeanFlow Geng et al. [2025a,b], which learns an averaged velocity field $u_{t \rightarrow r}(x) = \frac{\psi_{t \rightarrow r}(x) - x}{r-t}$ to parameterize the flow map. Despite these efforts, introducing reliable dataset-level supervision for long-range flow maps remains challenging in practice, as summarized below.

Challenge 2.4 (Challenge for Flow-Map Methods). *A key challenge in flow-map learning is how to introduce dataset-level supervision for long-range maps $\psi_{t \rightarrow r}$ with large $r - t$. Progressive-extension methods do not directly use dataset supervision for long-horizon maps, and instead rely on indirect signals propagated from short-horizon maps through the semigroup constraint. Continuous-based methods inject supervision via the instantaneous conditional velocity in the limiting continuous equation, but they typically require differentiating through the map, which may hurt training stability and substantially increase computational cost.*

3 Long-Short Flow-Map Perspective

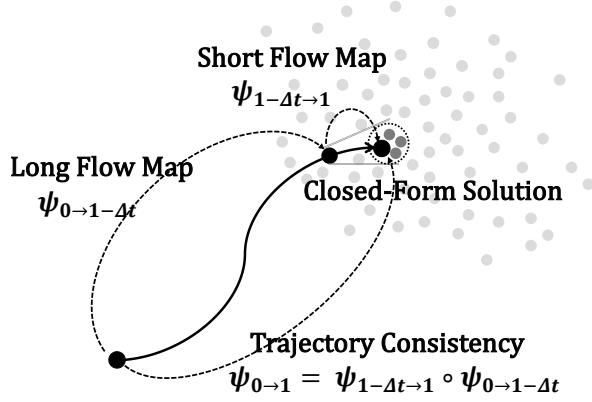


Figure 2: **Overview of the Long-Short Flow Map framework.** Leveraging flow-map trajectory consistency, we decompose the full map $\psi_{0 \rightarrow 1}$ into a long map $\psi_{0 \rightarrow 1 - \Delta t}$ and a short map $\psi_{1 - \Delta t \rightarrow 1}$. The short map is approximated using forward Euler or the trapezoidal rule and then computed via the closed-form solution in flow matching, providing dataset-level supervision for learning the long map $\psi_{0 \rightarrow 1 - \Delta t}$. Taking the limit $\Delta t \rightarrow 0$ yields a long-short flow-map derivation of the Drifting Model.

As discussed above, both the closed-form Flow Matching and flow-map approaches face practical challenges. The closed-form optimal velocity becomes impractical to evaluate when t is far from the terminal time 1, while flow-map learning struggles to obtain a dataset-level supervision when enforcing trajectory consistency. Our key insight is that these two approaches can be combined via a long-short decomposition of flow maps, so that each mitigates the other's limitations. As in flow-map methods, we aim to learn $\psi_{t \rightarrow \tau}$. Using the trajectory-consistency property in Proposition 2.3, we start from the composition identity $\psi_{0 \rightarrow 1} = \psi_{1 - \Delta t \rightarrow 1} \circ \psi_{0 \rightarrow 1 - \Delta t}$. We use the short flow map $\psi_{1 - \Delta t \rightarrow 1}$ for a small terminal step near the endpoint, and the long flow map $\psi_{0 \rightarrow 1 - \Delta t}$ for the main large-step transport from noise toward data. We refer to this factorization as the **long-short flow-map decomposition** (as shown in Figure 2). The main idea is to use the flow-matching closed-form solution to approximate the short terminal map $\psi_{1 - \Delta t \rightarrow 1}$, where the closed-form solution is accurate and computationally tractable, thereby providing a dataset-tied supervisory signal for learning the remaining long map $\psi_{0 \rightarrow 1 - \Delta t}$ through trajectory consistency. This coupling simultaneously alleviates the two challenges we mentioned above, effectively unifying the one-step flow map with the closed-form flow matching. We detail the derivation below.

3.1 First-Order Approximation

For $\psi_{0 \rightarrow 1}^\theta(x_0) = \psi_{1 - \Delta t \rightarrow 1}^\theta(\psi_{0 \rightarrow 1 - \Delta t}^\theta(x_0))$, let $x_{1 - \Delta t}^\theta = \psi_{0 \rightarrow 1 - \Delta t}^\theta(x_0)$. Using a **first-order forward Euler approximation** for the short interval $[1 - \Delta t, 1]$ via the instantaneous velocity field $u_t(\cdot)$, we obtain $\psi_{1 - \Delta t \rightarrow 1}^\theta(x_{1 - \Delta t}^\theta) \approx x_{1 - \Delta t}^\theta + \Delta t u_{1 - \Delta t}(x_{1 - \Delta t}^\theta)$. Substituting this approximation back into the consistency equation yields

$$\psi_{0 \rightarrow 1}^\theta(x_0) \approx \psi_{0 \rightarrow 1 - \Delta t}^\theta(x_0) + \Delta t u_{1 - \Delta t}(x_{1 - \Delta t}^\theta). \quad (9)$$

Therefore, to learn the terminal flow map $\psi_{0 \rightarrow 1}^\theta(x_0)$, we can consider an objective that enforces the above relation

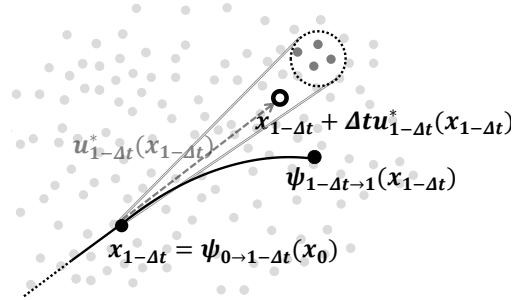
$$\mathcal{L}(\theta) = \mathbb{E}_{x_0 \sim p_0} \left[\left\| \psi_{0 \rightarrow 1}^\theta(x_0) - sg(\psi_{0 \rightarrow 1 - \Delta t}^\theta(x_0) + \Delta t u_{1 - \Delta t}(x_{1 - \Delta t}^\theta)) \right\|^2 \right], \quad (10)$$

We mollify the kernel $k_t(y, x)$ as

$$k_t^\epsilon(y, x) = e^{-\frac{\|ty - x\|^2}{2(1-t)^2 + \epsilon}} \quad (11)$$

to avoid singular behavior near $t = 1$, and now adopt the closed-form solution in Equation 5 for the instantaneous velocity at $t = 1 - \Delta t$ to obtain

$$\begin{aligned} \mathcal{L}(\theta) &= \mathbb{E}_{x_0 \sim p_0} \left[\left\| \psi_{0 \rightarrow 1}^\theta(x_0) - sg(\psi_{0 \rightarrow 1 - \Delta t}^\theta(x_0) + \Delta t u_{1 - \Delta t}(x_{1 - \Delta t}^\theta)) \right\|^2 \right] \\ &= \mathbb{E}_{x_0 \sim p_0} \left[\left\| \psi_{0 \rightarrow 1}^\theta(x_0) - sg\left(\psi_{0 \rightarrow 1 - \Delta t}^\theta(x_0) + \Delta t \frac{\mathbb{E}_{x_1 \sim p_1} \left[\frac{x_1 - x_{1 - \Delta t}^\theta}{1 - (1 - \Delta t)} k_{1 - \Delta t}^\epsilon(x_1, x_{1 - \Delta t}^\theta) \right]}{\mathbb{E}_{x_1 \sim p_1} [k_{1 - \Delta t}^\epsilon(x_1, x_{1 - \Delta t}^\theta)]} \right) \right\|^2 \right] \\ &= \mathbb{E}_{x_0 \sim p_0} \left[\left\| \psi_{0 \rightarrow 1}^\theta(x_0) - sg\left(\psi_{0 \rightarrow 1 - \Delta t}^\theta(x_0) + \frac{\mathbb{E}_{x_1 \sim p_1} [(x_1 - \psi_{0 \rightarrow 1 - \Delta t}^\theta(x_0)) k_{1 - \Delta t}^\epsilon(x_1, \psi_{0 \rightarrow 1 - \Delta t}^\theta(x_0))]}{\mathbb{E}_{x_1 \sim p_1} [k_{1 - \Delta t}^\epsilon(x_1, \psi_{0 \rightarrow 1 - \Delta t}^\theta(x_0))]} \right) \right\|^2 \right] \end{aligned} \quad (12)$$



Then let $\Delta t \rightarrow 0$, we have

$$\mathcal{L}(\theta) = \mathbb{E}_{x_0 \sim p_0} \left[\left\| \psi_{0 \rightarrow 1}^\theta(x_0) - \text{sg}(\psi_{0 \rightarrow 1}^\theta(x_0)) + \frac{\mathbb{E}_{x_1 \sim p_1} [(x_1 - \psi_{0 \rightarrow 1}^\theta(x_0)) k_1^\epsilon(x_1, \psi_{0 \rightarrow 1}^\theta(x_0))]}{\mathbb{E}_{x_1 \sim p_1} [k_1^\epsilon(x_1, \psi_{0 \rightarrow 1}^\theta(x_0))]} \right\|^2 \right] \quad (13)$$

where $k_1^\epsilon(y, x) = e^{-\frac{\|y-x\|^2}{\epsilon}}$. This loss involves only a single learnable map $\psi_{0 \rightarrow 1}^\theta$, and therefore can be used to directly train $\psi_{0 \rightarrow 1}^\theta$. During training, the expectations in Equation 13 are estimated by Monte Carlo using samples within each mini-batch. Once learned, it naturally yields a one-step generator by sampling $x_0 \sim p_0$ and computing $\psi_{0 \rightarrow 1}^\theta(x_0)$.

In this loss, the residual term $\mathcal{R}(\theta) \triangleq \frac{\mathbb{E}_{x_1 \sim p_1} [(x_1 - \psi_{0 \rightarrow 1}^\theta(x_0)) k_1^\epsilon(x_1, \psi_{0 \rightarrow 1}^\theta(x_0))]}{\mathbb{E}_{x_1 \sim p_1} [k_1^\epsilon(x_1, \psi_{0 \rightarrow 1}^\theta(x_0))]}$ is induced by the closed-form solution associated with an infinitesimally short terminal map $\psi_{1-\Delta t \rightarrow 1}^\theta$ as $\Delta t \rightarrow 0$, and it serves as an effective supervisory signal for learning the long map $\psi_{0 \rightarrow 1-\Delta t}^\theta$. According to our derivation, when $\psi_{0 \rightarrow 1}^\theta(x_0)$ matches the desired transport, the model output and the $\text{sg}(\cdot)$ target coincide, and $\mathcal{R}(\theta)$ attains its optimum. Moreover, $\mathcal{R}(\theta)$ admits a concrete interpretation: it is a regression-optimal, kernel-weighted conditional expectation that quantifies the discrepancy between the generated point $\psi_{0 \rightarrow 1}^\theta(x_0)$ and the target distribution p_1 , and the loss minimizes this discrepancy in the least-squares sense.

3.2 Second-Order Approximation

In the discussion above, we approximated the short flow map using a first-order forward Euler method and then applied the closed-form solution. To obtain a more accurate estimation, here we instead use a second-order trapezoidal rule to approximate the evolution over $[1 - \Delta t, 1]$.

$$\psi_{0 \rightarrow 1}^\theta(x_0) \approx \psi_{0 \rightarrow 1-\Delta t}^\theta(x_0) + \frac{\Delta t}{2} (u_{1-\Delta t}(\psi_{0 \rightarrow 1-\Delta t}^\theta(x_0)) + u_{1-}(\psi_{0 \rightarrow 1}^\theta(x_0))). \quad (14)$$

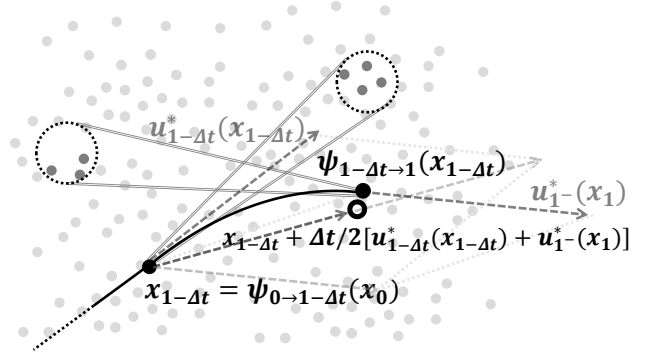
As in Equation 12, we use the Flow Matching closed-form solution for the velocity on the interval $[1 - \Delta t, 1]$. The main technical issue is that we require a closed-form expression for the endpoint velocity $u_{1-} = \lim_{t \rightarrow 1-} u_t$, which is given by the following theorem.

Theorem 3.1 (Closed-Form Solution of the Endpoint Velocity). *For Flow Matching, under mild smoothness assumptions on the underlying distributions, the optimal velocity satisfies $\lim_{t \rightarrow 1-} u_t^*(x) = x$. Consequently, the left-limit endpoint velocity $u_{1-}^*(x) \triangleq \lim_{t \rightarrow 1-} u_t^*(x)$ admits the closed form for any $t \in [0, 1]$*

$$u_{1-}^*(x) = \mathbb{E}_{x_t \sim p_{t|1}(x_t|x)} \left[\frac{x - x_t}{1 - t} \right] = \frac{\mathbb{E}_{x_t \sim p_t} \left[\frac{x - x_t}{1 - t} k_t(x, x_t) \right]}{\mathbb{E}_{x_t \sim p_t} [k_t(x, x_t)]} \quad (15)$$

see subsection A.3 for proof.

In the above formulation, p_t does not admit a closed-form expression. We therefore approximate it using samples pushed forward by the learned long flow map, i.e., $x_t \approx \psi_{0 \rightarrow t}^\theta(x_0)$ with $x_0 \sim p_0$. Moreover, although the theorem states $\lim_{t \rightarrow 1-} u_t^*(x) = x$, directly setting $u_{1-}(x) = x$ is insufficient: it does not cancel the Δt terms (which is crucial in the derivation of Equation 12) and it cannot reflect the discrepancy between p_t and p_1 . We therefore adopt the Flow



Matching closed-form solution of the instantaneous velocity $u_{1-\Delta t}$ and u_{1-} at $t = 1 - \Delta t$ and $t = 1$

$$\begin{aligned}
 \mathcal{L}(\theta) &= \mathbb{E}_{x_0 \sim p_0} \left[\left\| \psi_{0 \rightarrow 1}^\theta(x_0) - \text{sg}(\psi_{0 \rightarrow 1-\Delta t}^\theta(x_0) + \frac{1}{2} \Delta t u_{1-\Delta t}(x_{1-\Delta t}^\theta) + \frac{1}{2} \Delta t u_{1-}(x_1^\theta)) \right\|^2 \right] \\
 &= \mathbb{E}_{x_0 \sim p_0} \left[\left\| \psi_{0 \rightarrow 1}^\theta(x_0) - \text{sg}(\psi_{0 \rightarrow 1-\Delta t}^\theta(x_0) + \frac{1}{2} \Delta t \frac{\mathbb{E}_{x_1 \sim p_1} \left[\frac{x_1 - \psi_{0 \rightarrow 1-\Delta t}^\theta(x_0)}{1 - (1-\Delta t)} k_{1-\Delta t}^\epsilon(x_1, \psi_{0 \rightarrow 1-\Delta t}^\theta(x_0)) \right]}{\mathbb{E}_{x_1 \sim p_1} [k_{1-\Delta t}^\epsilon(x_1, \psi_{0 \rightarrow 1-\Delta t}^\theta(x_0))]} \right. \right. \\
 &\quad \left. \left. + \frac{1}{2} \Delta t \frac{\mathbb{E}_{x_{1-\Delta t}^\theta \sim p_{1-\Delta t}^\theta} \left[\frac{\psi_{0 \rightarrow 1}^\theta(x_0) - x_{1-\Delta t}^\theta}{1 - (1-\Delta t)} k_{1-\Delta t}^\epsilon(\psi_{0 \rightarrow 1}^\theta(x_0), x_{1-\Delta t}^\theta) \right]}{\mathbb{E}_{x_{1-\Delta t}^\theta \sim p_{1-\Delta t}^\theta} [k_{1-\Delta t}^\epsilon(\psi_{0 \rightarrow 1}^\theta(x_0), x_{1-\Delta t}^\theta)]} \right\|^2 \right] \\
 &= \mathbb{E}_{x_0 \sim p_0} \left[\left\| \psi_{0 \rightarrow 1}^\theta(x_0) - \text{sg}(\psi_{0 \rightarrow 1-\Delta t}^\theta(x_0) + \frac{1}{2} \frac{\mathbb{E}_{x_1 \sim p_1} [(x_1 - \psi_{0 \rightarrow 1-\Delta t}^\theta(x_0)) k_{1-\Delta t}^\epsilon(x_1, \psi_{0 \rightarrow 1-\Delta t}^\theta(x_0))]}{\mathbb{E}_{x_1 \sim p_1} [k_{1-\Delta t}^\epsilon(x_1, \psi_{0 \rightarrow 1-\Delta t}^\theta(x_0))]} \right. \right. \\
 &\quad \left. \left. + \frac{1}{2} \frac{\mathbb{E}_{x_{1-\Delta t}^\theta \sim p_{1-\Delta t}^\theta} [(\psi_{0 \rightarrow 1}^\theta(x_0) - x_{1-\Delta t}^\theta) k_{1-\Delta t}^\epsilon(\psi_{0 \rightarrow 1}^\theta(x_0), x_{1-\Delta t}^\theta)]}{\mathbb{E}_{x_{1-\Delta t}^\theta \sim p_{1-\Delta t}^\theta} [k_{1-\Delta t}^\epsilon(\psi_{0 \rightarrow 1}^\theta(x_0), x_{1-\Delta t}^\theta)]} \right\|^2 \right] \tag{16}
 \end{aligned}$$

where we denote the distribution of $x_{1-\Delta t}^\theta = \psi_{0 \rightarrow 1-\Delta t}^\theta(x_0')$, $x_0' \sim p_0$ as $x_{1-\Delta t}^\theta \sim p_{1-\Delta t}^\theta$. Then let $\Delta t \rightarrow 0$, we have

$$\begin{aligned}
 \mathcal{L}(\theta) &= \mathbb{E}_{x_0 \sim p_0} \left[\left\| \psi_{0 \rightarrow 1}^\theta(x_0) - \text{sg}(\psi_{0 \rightarrow 1}^\theta(x_0) + \frac{1}{2} \frac{\mathbb{E}_{x_1 \sim p_1} [(x_1 - \psi_{0 \rightarrow 1}^\theta(x_0)) k_1^\epsilon(x_1, \psi_{0 \rightarrow 1}^\theta(x_0))]}{\mathbb{E}_{x_1 \sim p_1} [k_1^\epsilon(x_1, \psi_{0 \rightarrow 1}^\theta(x_0))]} \right. \right. \\
 &\quad \left. \left. + \frac{1}{2} \frac{\mathbb{E}_{x_1^\theta = \psi_{0 \rightarrow 1}^\theta(x_0'), x_0' \sim p_0} [(\psi_{0 \rightarrow 1}^\theta(x_0) - x_1^\theta) k_1^\epsilon(\psi_{0 \rightarrow 1}^\theta(x_0), x_1^\theta)]}{\mathbb{E}_{x_1^\theta = \psi_{0 \rightarrow 1}^\theta(x_0'), x_0' \sim p_0} [k_1^\epsilon(\psi_{0 \rightarrow 1}^\theta(x_0), x_1^\theta)]} \right\|^2 \right] \tag{17}
 \end{aligned}$$

In this loss, the trapezoidal-rule approximation of the short flow map provides a more accurate supervisory signal for learning the long flow map. Compared to the first-order Euler-based objective in Equation 13, the key difference lies in the residual term: it is no longer a point-to-distribution regression target between point $\psi_{0 \rightarrow 1}^\theta(x_0)$ and distribution p_1 , but rather a discrepancy between two distributions $p_{1-\Delta t}^\theta$ and p_1 estimated from samples $\psi_{0 \rightarrow 1}^\theta(x_0)$. As a result, when the flow map is optimal, the residual does not merely attain a regression-optimal value; it becomes exactly zero.

3.3 Connection with Drifting Model

In the derivation above, we use the long-short flow-map decomposition to combine flow-map learning with the Flow-Matching closed-form solution: the closed-form solution on the short flow map provides a dataset-tied supervisory signal, enabling learning the long flow map and yielding a one-step map $\psi_{0 \rightarrow 1}^\theta$. From this perspective, the objectives in Equation 13 and Equation 17 recover the losses used in the Drifting Model Deng et al. [2026]. This connection provides a principled derivation of the Drifting Model and enables intuitive explanations of its key design choices. We first summarize the Drifting Model and then elaborate on its connection to our derivation by showing how its training objectives and design choices naturally arise from the long-short flow-map viewpoint.

Drifting Model The Drifting Model Deng et al. [2026] directly learns a one-step mapping $f^\theta : \mathcal{X} \rightarrow \mathcal{X}$ that pushes forward noise to data, i.e., $f^\theta(\epsilon) \sim q_\theta$ with $\epsilon \sim p_0$, and aims to match q_θ to $p_1 = p_{\text{data}}$. The main idea is to make the pushforward distribution progressively closer to the target distribution during training. Specifically, the method introduces a drift field $V_{p_1, q_\theta} : \mathcal{X} \rightarrow \mathcal{X}$ that corrects samples from q_θ toward p_1 and ideally satisfies $x + V_{p, q_\theta}(x) \sim p_1$ when $x \sim q_\theta$. Training then encourages $f^\theta(\epsilon)$ to agree with its drift-corrected counterpart:

$$\mathcal{L}(\theta) = \mathbb{E}_{\epsilon \sim p_0} \left[\left\| f^\theta(\epsilon) - \text{sg}(f^\theta(\epsilon) + V_{p_1, q_\theta}(f^\theta(\epsilon))) \right\|_2^2 \right], \tag{18}$$

where q_θ denotes the distribution induced by $f^\theta(\epsilon)$.

For $V_{p, q}$ that incorporates supervision from the target data distribution, the Drifting Model adopts a kernel-based construction with an attraction-repulsion structure:

$$\begin{aligned}
 V_{p, q}(x) &= V_p^+(x) - V_q^-(x), \\
 V_p^+(x) &= \frac{\mathbb{E}_{y \sim p} [k(x, y)(y - x)]}{\mathbb{E}_{y \sim p} [k(x, y)]}, \\
 V_q^-(x) &= \frac{\mathbb{E}_{y \sim q} [k(x, y)(y - x)]}{\mathbb{E}_{y \sim q} [k(x, y)]}, \tag{19}
 \end{aligned}$$

where $k(x, y)$ is a similarity kernel (implemented via a Laplacian kernel $e^{-\|y-x\|/\epsilon}$ in practice). Ideally, this definition satisfies a consistency condition: $V_{p,q}(x) = 0$ whenever $p = q$, so that no correction is applied when the two distributions coincide.

Connection of Loss Functions We observe that the loss in Equation 13 obtained by approximating the short terminal evolution via a first-order forward Euler step coincides with the Drifting Model objective that uses the attraction-only drift field $V_{p,q}(x) = V_p^+(x)$ for the drifting loss in Equation 18, where

$$f^\theta := \psi_{0 \rightarrow 1}^\theta, \quad V_{p_1, p_1^\theta} = V_{p_1}^+, \quad V_{p_1}^+(x) = \frac{\mathbb{E}_{x_1 \sim p_1}[(x_1 - x)k_1(x_1, x)]}{\mathbb{E}_{x_1 \sim p_1}[k_1(x_1, x)]} \quad (20)$$

In contrast, the loss in Equation 17 derived from a second-order trapezoidal approximation over the same short interval matches the Drifting Model objective with the attraction-repulsion drift field $V_{p,q}(x) = V_p^+(x) - V_q^-(x)$, where

$$f^\theta := \psi_{0 \rightarrow 1}^\theta, \quad V_{p_1, p_1^\theta} = V_{p_1}^+ - V_{p_1^\theta}^-, \quad V_{p_1}^+(x) = \frac{\mathbb{E}_{x_1 \sim p_1}[(x_1 - x)k_1(x_1, x)]}{\mathbb{E}_{x_1 \sim p_1}[k_1(x_1, x)]}, \quad V_{p_1^\theta}^-(x) = \frac{\mathbb{E}_{x_1 \sim p_1^\theta}[(x_1 - x)k_1(x, x_1)]}{\mathbb{E}_{x_1 \sim p_1^\theta}[k_1(x, x_1)]} \quad (21)$$

Discussion on Design Choices The connection between the loss functions yields the following insights regarding several design choices of the Drifting Model, which we will discuss briefly below.

1. **Interpretation.** The Drifting Model can be viewed as learning a flow map via trajectory consistency, and then selecting the segment $s \rightarrow r$ in Proposition 2.3 to be a very short interval near the terminal time, i.e., $1 - \Delta t \rightarrow 1$. Over this short interval, it directly applies the closed-form solution of Flow Matching to obtain supervision from the dataset.
2. **Why $V^+ - V^-$ emerges and why it helps.** If the estimation over $1 - \Delta t \rightarrow 1$ uses a first-order forward Euler method, one recovers the original Drifting Model form that involves only V^+ . In contrast, if a second-order trapezoidal rule is used, the derivation naturally yields the balanced attraction-repulsion form $V^+ - V^-$. Since the learned flow map is generally not optimal, the terminal interval $1 - \Delta t \rightarrow 1$ remains affected by approximation error even as $\Delta t \rightarrow 0$. Therefore, the order of the terminal-interval estimator provides a principled explanation for why the symmetric correction $V^+ - V^-$ tends to outperform the one-sided variant V^+ , as well as other imbalanced choices such as $3V^+ - V^-$.
3. **Kernel Selection.** As revealed by the proofs of subsection A.1 and subsection A.3, the kernel $k_t(x, y)$ adopted in Equation 13 and Equation 17 is tightly coupled with the form of the initial noise distribution p_0 . In particular, when we choose Gaussian noise, the resulting kernel naturally becomes the squared-exponential Gaussian kernel $e^{-|y-x|^2/\epsilon}$. Importantly, our framework does not restrict the choice of p_0 , and therefore does not constrain the kernel family in Equation 13 and Equation 17 either. For example, by choosing p_0 to follow a Laplace distribution, we recover the Laplacian kernel $e^{-|y-x|/\epsilon}$ used in the original Drifting Model Deng et al. [2026]. More broadly, relating kernel design to the choice of initial noise indicates a connection between these two components. This connection hints that recent advances in initial-noise optimization, such as blue-noise sampling strategies Huang et al. [2024], could be incorporated to refine the kernel selections in Equation 13 and Equation 17. A systematic investigation of this direction remains open.

In Appendix C, we discuss classifier-free guidance (CFG), which Deng et al. [2026] identifies as a key distinction between Drifting Model and distribution moment matching Li et al. [2015], Dziugaite et al. [2015] (see the related-work discussion in section 7).

4 Application: Likelihood Learning

Here we leverage the long-short flow-map perspective to derive a new objective for learning data likelihoods.

4.1 Background

For one-step generative methods based on flow maps, one can in principle compute the likelihood using the learned map $\psi_{t \rightarrow r}(x)$ via the change-of-variables formula $\log p_r(x_r) = \log p_t(x_t) - \log \left| \det \frac{\partial \psi_{t \rightarrow r}(x)}{\partial x} \right|_{x=x_t}$, where $x_r = \psi_{t \rightarrow r}(x_t)$. However, this requires evaluating the Jacobian determinant of the flow map, which does not scale to high-dimensional data. To address this issue, Ai et al. [2025] proposes to jointly learn, together with the flow

map $\psi_{t \rightarrow r}^\theta(x)$, an auxiliary model $D_{t \rightarrow r}^\theta(x)$ that predicts the average likelihood change from time t to r , namely $D_{t \rightarrow r}^\theta(x) = \frac{\log p_r(\psi_{t \rightarrow r}^\theta(x)) - \log p_t(x)}{r-t}$. Concretely, the evolution of the log-likelihood quantity $\log p_r(\psi_{t \rightarrow r}^\theta(x))$ satisfies

$$\frac{\partial \log p_r(\psi_{t \rightarrow r}^\theta(x))}{\partial r} = -\nabla \cdot u_r(y)|_{y=\psi_{t \rightarrow r}^\theta(x)} \quad (22)$$

and $D_{t \rightarrow r}^\theta(x)$ satisfies a trajectory consistency property $(r-t)D_{t \rightarrow r}^\theta(x_t) = (r-s)D_{s \rightarrow r}^\theta(x_s) + (s-t)D_{t \rightarrow s}^\theta(x_t)$, where $x_s = \psi_{t \rightarrow s}^\theta(x_t)$ for arbitrary $t < s < r$. Using this trajectory consistency and the evolution Equation 22 as a boundary condition $D_{t \rightarrow t}^\theta(x) = -\nabla \cdot u_t(x)$, Ai et al. [2025] learns $D_{t \rightarrow r}^\theta(x)$ jointly with the flow map $\psi_{t \rightarrow r}^\theta$. With the learned $D_{t \rightarrow r}^\theta(x)$, for any generated sample $x_1 = \psi_{0 \rightarrow 1}^\theta(x_0)$, one can efficiently obtain its likelihood $\log p_1(x_1) = \log p_0(x_0) + D_{0 \rightarrow 1}^\theta(x_0)$.

4.2 Drifting Model for Likelihood Learning

We aim to derive an analogous likelihood-learning objective for the Drifting Model under our flow-map perspective. Different from Ai et al. [2025], our goal is to learn the Eulerian log-likelihood change $G_{t \rightarrow r}^\theta(x) = \log p_r(x) - \log p_t(x)$. When combined with the flow map $\psi_{t \rightarrow r}^\theta$, the composed quantity $G_{t \rightarrow r}^\theta(\psi_{t \rightarrow r}^\theta(x))$ can also play a Lagrangian role. In the Eulerian view, $\log p_t(x)$ satisfies the following evolution equation

$$\frac{\partial}{\partial t} \log p_t(x) = -\nabla \log p_t(x) \cdot u_t(x) - \nabla \cdot u_t(x) \quad (23)$$

Because $G_{t \rightarrow r}^\theta(x) = \log p_r(x) - \log p_t(x)$, it satisfies the evolution equation $\frac{\partial}{\partial r} G_{t \rightarrow r}^\theta(x) = -\nabla \log p_r(x) \cdot u_r(x) - \nabla \cdot u_r(x)$ and the consistency relation $G_{t \rightarrow r}^\theta(x) = G_{s \rightarrow r}^\theta(x) + G_{t \rightarrow s}^\theta(x)$ for arbitrary $t < s < r$. Following the same idea as before, we apply this relation on $[0, 1]$ with a split point $1 - \Delta t$, namely $G_{0 \rightarrow 1}^\theta(x) = G_{0 \rightarrow 1 - \Delta t}^\theta(x) + G_{1 - \Delta t \rightarrow 1}^\theta(x)$ and approximate $G_{1 - \Delta t \rightarrow 1}^\theta(x)$ by the trapezoidal rule. For the learned flow map $\psi_{t \rightarrow r}^\theta(x)$ and the learned likelihood change $G_{t \rightarrow r}^\theta(x)$, we enforce that they satisfy

$$G_{0 \rightarrow 1}^\theta(x) \approx G_{0 \rightarrow 1 - \Delta t}^\theta(x) - \frac{\Delta t}{2} (\nabla \log p_{1 - \Delta t}^\theta(x) u_{1 - \Delta t}(x) + \nabla \log p_1^\theta(x) u_{1-}(x) + \nabla \cdot u_{1-}(x) + \nabla \cdot u_{1 - \Delta t}(x)) \quad (24)$$

where $p_t^\theta(x) = p_0(x)e^{G_{0 \rightarrow t}^\theta(x)}$. Here, we need to compute the divergence terms $\nabla \cdot u_{1 - \Delta t}$ and $\nabla \cdot u_{1-}$, whose evaluation is provided by the following theorem.

Theorem 4.1 (Closed-Form Solution for Velocity Divergence). *For the closed-form solution of the velocity field $u_t^*(x)$ in Equation 5 and the endpoint velocity $u_{1-}^*(x)$ in Equation 15 with the mollified kernel k_t^ϵ in Equation 11, their divergences can be also computed in closed form as*

$$\begin{aligned} \nabla \cdot u_t^*(x) &= \frac{1}{1-t} \left[\frac{2t}{2(1-t)^2 + \epsilon} \left(\frac{\mathbb{E}_{x_1 \sim p_1} [\|x_1\|^2 k_t^\epsilon(x_1, x)]}{\mathbb{E}_{x_1 \sim p_1} [k_t^\epsilon(x_1, x)]} - \left\| \frac{\mathbb{E}_{x_1 \sim p_1} [x_1 k_t^\epsilon(x_1, x)]}{\mathbb{E}_{x_1 \sim p_1} [k_t^\epsilon(x_1, x)]} \right\|^2 \right) - d \right] \\ \nabla \cdot u_{1-}^*(x) &= \frac{1}{1-t} \left[d - \frac{2t^2}{2(1-t)^2 + \epsilon} \left(\frac{\mathbb{E}_{x_t \sim p_t} [\|x_t\|^2 k_t^\epsilon(x, x_t)]}{\mathbb{E}_{x_t \sim p_t} [k_t^\epsilon(x, x_t)]} - \left\| \frac{\mathbb{E}_{x_t \sim p_t} [x_t k_t^\epsilon(x, x_t)]}{\mathbb{E}_{x_t \sim p_t} [k_t^\epsilon(x, x_t)]} \right\|^2 \right) \right] \end{aligned} \quad (25)$$

See subsection A.4 for the proof.

Therefore, $G_{0 \rightarrow 1}^\theta(x)$ can be calculated as

$$\begin{aligned} G_{0 \rightarrow 1}^\theta(x) &= G_{0 \rightarrow 1 - \Delta t}^\theta(x) - \frac{\Delta t}{2} (\nabla \log p_{1 - \Delta t}^\theta(x) \cdot u_{1 - \Delta t}(x) + \nabla \log p_1^\theta(x) \cdot u_{1-}(x) + \nabla \cdot u_{1-}(x) + \nabla \cdot u_{1 - \Delta t}(x)) \\ &= G_{0 \rightarrow 1 - \Delta t}^\theta(x) - \frac{1}{2} (\nabla \log p_{1 - \Delta t}^\theta(x) \frac{\mathbb{E}_{x_1 \sim p_1} [(x_1 - x) k_{1 - \Delta t}^\epsilon(x_1, x)]}{\mathbb{E}_{x_1 \sim p_1} [k_{1 - \Delta t}^\epsilon(x_1, x)]} \\ &\quad + \nabla \log p_1^\theta(x) \cdot \frac{\mathbb{E}_{x_{1 - \Delta t} \sim p_{1 - \Delta t}} [(x - x_{1 - \Delta t}) k_{1 - \Delta t}^\epsilon(x, x_{1 - \Delta t})]}{\mathbb{E}_{x_{1 - \Delta t} \sim p_{1 - \Delta t}} [k_{1 - \Delta t}^\epsilon(x, x_{1 - \Delta t})]} \\ &\quad - \frac{(1 - \Delta t)}{2\Delta t^2 + \epsilon} \left(\frac{\mathbb{E}_{x_1 \sim p_1} [\|x_1\|^2 k_{1 - \Delta t}^\epsilon(x_1, x)]}{\mathbb{E}_{x_1 \sim p_1} [k_{1 - \Delta t}^\epsilon(x_1, x)]} - \left\| \frac{\mathbb{E}_{x_1 \sim p_1} [x_1 k_{1 - \Delta t}^\epsilon(x_1, x)]}{\mathbb{E}_{x_1 \sim p_1} [k_{1 - \Delta t}^\epsilon(x_1, x)]} \right\|^2 \right) \\ &\quad + \frac{(1 - \Delta t)^2}{2\Delta t^2 + \epsilon} \left(\frac{\mathbb{E}_{x_{1 - \Delta t} \sim p_{1 - \Delta t}} [\|x_{1 - \Delta t}\|^2 k_{1 - \Delta t}^\epsilon(x, x_{1 - \Delta t})]}{\mathbb{E}_{x_{1 - \Delta t} \sim p_{1 - \Delta t}} [k_{1 - \Delta t}^\epsilon(x, x_{1 - \Delta t})]} - \left\| \frac{\mathbb{E}_{x_{1 - \Delta t} \sim p_{1 - \Delta t}} [x_{1 - \Delta t} k_{1 - \Delta t}^\epsilon(x, x_{1 - \Delta t})]}{\mathbb{E}_{x_{1 - \Delta t} \sim p_{1 - \Delta t}} [k_{1 - \Delta t}^\epsilon(x, x_{1 - \Delta t})]} \right\|^2 \right) \end{aligned} \quad (26)$$

In the above expression, since $p_{1-\Delta t}$ is unknown, we instead draw samples from $p_{1-\Delta t}^\theta$ induced by $G_{0 \rightarrow 1-\Delta t}^\theta$; the sampling procedure is described in subsection 4.3. Letting $\Delta t \rightarrow 0$, we obtain the loss

$$\begin{aligned} \mathcal{L}(\theta) = & \mathbb{E}_{x \sim p_{\text{sample}}} \left[\left\| G_{0 \rightarrow 1}^\theta(x) - \text{sg}(G_{0 \rightarrow 1}^\theta(x)) - \frac{1}{2} \nabla G_{0 \rightarrow 1}^\theta(x) \left(\frac{\mathbb{E}_{x_1 \sim p_1} [x_1 k_1^\epsilon(x_1, x)]}{\mathbb{E}_{x_1 \sim p_1} [k_1^\epsilon(x_1, x)]} - \frac{\mathbb{E}_{x_1 \sim p_1^\theta} [x_1 k_1^\epsilon(x_1, x)]}{\mathbb{E}_{x_1 \sim p_1^\theta} [k_1^\epsilon(x_1, x)]} \right) \right. \right. \\ & \left. \left. - \frac{1}{\epsilon} \left(\frac{\mathbb{E}_{x_1 \sim p_1} [\|x_1\|^2 k_1^\epsilon(x_1, x)]}{\mathbb{E}_{x_1 \sim p_1} [k_1^\epsilon(x_1, x)]} - \left\| \frac{\mathbb{E}_{x_1 \sim p_1} [x_1 k_1^\epsilon(x_1, x)]}{\mathbb{E}_{x_1 \sim p_1} [k_1^\epsilon(x_1, x)]} \right\|^2 - \frac{\mathbb{E}_{x_1 \sim p_1^\theta} [\|x_1\|^2 k_1^\epsilon(x_1, x)]}{\mathbb{E}_{x_1 \sim p_1^\theta} [k_1^\epsilon(x_1, x)]} + \left\| \frac{\mathbb{E}_{x_1 \sim p_1^\theta} [x_1 k_1^\epsilon(x_1, x)]}{\mathbb{E}_{x_1 \sim p_1^\theta} [k_1^\epsilon(x_1, x)]} \right\|^2 \right) \right\|^2 \right] \end{aligned} \quad (27)$$

where p_{sample} specifies the region on which we want to learn the field. For example, if we aim to learn $G_{0 \rightarrow 1}^\theta(x)$ over a bounded set S , we can choose p_{sample} to be the uniform distribution on S . If we instead focus on points near the data manifold, we can set p_{sample} as a mixture of Gaussians centered at $\psi_{t \rightarrow r}^\theta(x_0)$ with $x_0 \sim p_0$.

In addition, to ensure that the learned likelihood satisfies the normalization constraint, we introduce a normalization loss

$$\mathcal{L}_{\text{norm}}(\theta) = \mathbb{E}_{x \sim p_{\text{sample}}} \left\| \mathbb{E}_{x_1 \sim p_1} [k_1^\epsilon(x_1, x)] - \mathbb{E}_{x_1 \sim p_1^\theta} [k_1^\epsilon(x_1, x)] \right\|^2 \quad (28)$$

As a result, the final training objective is given by $\mathcal{L}(\theta) + \lambda \mathcal{L}_{\text{norm}}(\theta)$ with hyperparameter λ . The expectations in Equation 27 and Equation 28 are approximated during training by mini-batch Monte Carlo estimates, as in the sample-generation losses in Equation 13 and Equation 17.

4.3 Sampling Process for Lagrangian Likelihood Learning

In the above formulation, we note that the expectation $\mathbb{E}_{x_1 \sim p_1^\theta}[\cdot]$ is required. Although $p_1^\theta(x) = p_0(x)e^{D_{0 \rightarrow 1}^\theta(x)}$, the model $D_{0 \rightarrow 1}^\theta(x_0)$ is not directly amenable to sampling. To address this issue, we adopt importance sampling, i.e.,

$$\mathbb{E}_{x_1 \sim p_1^\theta}[\dots] = \mathbb{E}_{x_1 \sim p_{\text{ref}}} \left[\dots \frac{p_0(x_1)e^{D_{0 \rightarrow 1}^\theta(x_1)}}{p_{\text{ref}}(x_1)} \right]. \quad (29)$$

Here, p_{ref} denotes a reference distribution from which we can efficiently sample and whose probability density function is available. Ideally, the support of p_{ref} should closely match that of p_1^θ .

In practice, we construct p_{ref} on a per-batch basis as a multimodal Gaussian mixture whose components are centered at the mini-batch samples $\{x_1^{(i)}\}_{i=1}^B$ drawn from the dataset. Specifically, we define

$$p_{\text{ref}}(x) = \frac{1}{B} \sum_{i=1}^B \mathcal{N}(x; x_1^{(i)}, \sigma^2 I). \quad (30)$$

where B denotes the batch size and σ controls the spread of each Gaussian component.

5 Open Problems in Feature-Space Optimization

For high-dimensional natural data, such as pixel-space generation, the Drifting Model may suffer from the curse of dimensionality. This issue arises because the training process is driven by the kernel $k_1^\epsilon(y, x)$, whose evaluation depends on pairwise distances. In high dimensions, standard distance metrics lose discriminative power. Distances concentrate and become nearly constant, which is a well-known manifestation of the dimensionality curse. As a result, the kernel weights become less informative and less stable. A natural remedy is to evaluate the kernel in a feature space where neighborhood structure is more meaningful, for example, a lower-dimensional space, or a feature space with stronger anisotropy and effectively lower intrinsic dimension. In such spaces, pairwise distances better reflect semantic similarity and yield more stable kernel weights. Motivated by this, Deng et al. [2026] proposes to compute the Drifting Model directly in feature space, leading to the following formulation:

$$\mathcal{L}(\theta) = \mathbb{E}_{\epsilon \sim p_0} \left[\left\| \phi_j(f^\theta(\epsilon)) - \text{sg}(\phi_j(f^\theta(\epsilon))) + [V_{\phi_j(p_1), \phi_j(q_\theta)}(\phi_j(f^\theta(\epsilon)))] \right\|^2 \right] \quad (31)$$

where $\phi_j(\cdot)$ denotes the j -th feature mapping, and $\phi_j(q_\theta)$ and $\phi_j(p_1)$ denote the pushforward distribution of q_θ and p_1 under ϕ_j , namely $\phi_j(f^\theta(x))$ with $x \sim p_0$ and $\phi_j(x)$ with $x \sim p_1$, respectively. Here, p_1 denotes the data distribution. The operator $V_{\phi_j(p), \phi_j(q_\theta)}(\phi_j(f^\theta(\epsilon)))$ is computed in the feature space $\mathcal{Z} = \phi_j(\mathcal{X})$. The collection $\{\phi_j\}_{j=1}^m$ is extracted from a pretrained, frozen encoder, and Deng et al. [2026] uses the encoder of MAE He et al. [2022]. In their implementation, m is on the order of several thousand.

We now interpret the Drifting Model in feature space and provide an intuitive explanation for why multiple feature maps are needed. Following the same decomposition of $\psi_{0 \rightarrow 1}$ as before, we apply it in the feature space induced by $\phi_j(\cdot)$ and linearize ϕ_j and approximate $\psi_{1-\Delta t \rightarrow 1}^\theta(x_{1-\Delta t}^\theta)$ using the trapezoidal rule as before:

$$\begin{aligned} \phi_j(\psi_{0 \rightarrow 1}^\theta(x_0)) &= \phi_j(\psi_{0 \rightarrow 1-\Delta t}^\theta(x_0) + \psi_{1-\Delta t \rightarrow 1}^\theta(x_{1-\Delta t}^\theta)) \\ &\approx \phi_j(\psi_{0 \rightarrow 1-\Delta t}^\theta(x_0)) + \frac{\Delta t}{2} [J_{\phi_j}(x_{1-\Delta t}^\theta)u_{1-\Delta t}(x_{1-\Delta t}^\theta) + J_{\phi_j}(x_1^\theta)u_{1-}(x_1^\theta)] \end{aligned} \quad (32)$$

where $J_{\phi_j}(x) = \frac{\partial \phi_j(x)}{\partial x}$ denotes the Jacobian of ϕ_j . Substituting the expressions of $u_{1-\Delta t}$ and u_{1-} into the above and taking $\Delta t \rightarrow 0$ yields the limiting loss

$$\begin{aligned} \mathcal{L}(\theta) &= \mathbb{E}_{x_0 \sim p_0} \left[\left\| \phi_j(\psi_{0 \rightarrow 1}^\theta(x_0)) - sg(\phi_j(\psi_{0 \rightarrow 1}^\theta(x_0)) + \frac{1}{2} J_{\phi_j}(\psi_{0 \rightarrow 1}^\theta(x_0)) \left(\frac{\mathbb{E}_{x_1 \sim p_1} [(x_1 - \psi_{0 \rightarrow 1}^\theta(x_0)) k_1^\epsilon(x_1, \psi_{0 \rightarrow 1}^\theta(x_0))]}{\mathbb{E}_{x_1 \sim p_1} [k_1^\epsilon(x_1, \psi_{0 \rightarrow 1}^\theta(x_0))]} \right. \right. \right. \\ &\quad \left. \left. \left. + \frac{\mathbb{E}_{x_1^\theta = \psi_{0 \rightarrow 1}^\theta(x_0'), x_0' \sim p_0} [(\psi_{0 \rightarrow 1}^\theta(x_0) - x_1^\theta) k_1^\epsilon(\psi_{0 \rightarrow 1}^\theta(x_0), x_1^\theta)]}{\mathbb{E}_{x_1^\theta = \psi_{0 \rightarrow 1}^\theta(x_0'), x_0' \sim p_0} [k_1^\epsilon(\psi_{0 \rightarrow 1}^\theta(x_0), x_1^\theta)]} \right) \right\|^2 \right] \end{aligned} \quad (33)$$

This expression characterizes the principled optimization direction for feature space. However, $\mathcal{L}(\theta)$ still relies on kernels computed in the original space \mathcal{X} , which limits its ability to reduce the effective dimensionality via ϕ_j .

Challenge 5.1 (Challenge of Feature-Space Optimization). *Although $\mathcal{L}(\theta)$ in Equation 33 provides a principled feature-space training objective, its kernel weights are still defined over \mathcal{X} rather than $\phi_j(\mathcal{X})$. As a result, the neighborhood structure used for weighting remains high-dimensional, and the expected mitigation of the curse of dimensionality from operating in feature space is not realized.*

In the derivations below, for convenience, we adopt the random-variable notation from Flow Matching. From the proofs in subsection A.1 and subsection A.3, we observe that the kernel weight k_t^ϵ in the closed-form optimal velocity comes from applying Flow Matching on p_1 with the linear conditional path $X_t = tX_1 + (1-t)X_0$, which implies $\frac{X_t - tX_1}{1-t} = X_0 \sim p_0$, where $X_1 \sim p_1$, $X_0 \sim p_0$, and $X_t \sim p_t$ are the random variables induced by the conditional probability path in Flow Matching. Therefore, if we want the kernel to be computed on $\phi_j(\mathcal{X})$, we should perform Flow Matching directly in that feature space.

Concretely, let $Z_1 = \phi_j(X_1) \in \mathcal{Z} = \phi_j(\mathcal{X})$ and denote its induced data distribution by $p_1^z(z) = \int_{\mathcal{X}} \mathbf{1}(z = \phi_j(x)) p_1(x) dx$. We consider a Gaussian reference distribution $Z_0 \sim p_0^z$ on \mathcal{Z} , and apply Flow Matching between p_0^z and p_1^z with the conditional path $Z_t = tZ_1 + (1-t)Z_0$. Then, for any $z = \phi_j(x)$, the optimal velocity in \mathcal{Z} is

$$\begin{aligned} u_t^{z,*}(z) &= \frac{\mathbb{E}_{z_1 \sim p_1^z} \left[\frac{z_1 - z}{1-t} k_t(z_1, z) \right]}{\mathbb{E}_{z_1 \sim p_1^z} [k_t(z_1, z)]} \\ u_{1-}^{z,*}(z) &= \frac{\mathbb{E}_{z_t \sim p_t^z} \left[\frac{z - z_t}{1-t} k_t(z, z_t) \right]}{\mathbb{E}_{z_t \sim p_t^z} [k_t(z, z_t)]} \end{aligned} \quad (34)$$

Here, $u_t^{z,*}$ and $u_{1-}^{z,*}$ involves kernel evaluation in feature space, which matches our goal. Next, we relate $u_t^{z,*}$ to Equation 32 and show how it can be incorporated into the estimator in Equation 32 to obtain a feature-space Drifting Model.

Theorem 5.2 (Feature-Data Space Optimal Velocity Relation). *Let $X_1 \sim p_1$ and define $Z_1 = \phi_j(X_1)$. Denote by $u_t^{x,*}(x)$ the optimal Flow Matching velocity in data space associated with the conditional path $X_t = tX_1 + (1-t)X_0$, and by $u_t^{z,*}(z)$ the optimal velocity in feature space associated with $Z_t = tZ_1 + (1-t)Z_0$, where X_0 and Z_0 are Gaussian reference variables on \mathcal{X} and \mathcal{Z} , respectively. We define $p_{x|z}(x|z)$ as the conditional distribution induced by the inverse of the deterministic map $z = \phi_j(x)$. Then, for $z = \phi_j(x)$, the two velocities satisfy the following approximate relations:*

$$\begin{aligned} u_t^{z,*}(z) &\approx J_{\phi_j}(x) \frac{\mathbb{E}[X_1 | Z_t = \phi_j(x)] - x}{1-t}, \\ u_{1-}^{z,*}(z) &\approx J_{\phi_j}(x) \frac{x - \mathbb{E}[X_t' | Z_1 = \phi_j(x)]}{1-t}, \end{aligned} \quad (35)$$

where $J_{\phi_j}(x) = \frac{\partial \phi_j(x)}{\partial x}$ is the Jacobian of ϕ_j , and X_t' is an auxiliary \mathcal{X} -valued random variable satisfying $\phi_j(X_t') = Z_t$ almost surely. The approximation \approx above follows from the first-order Taylor expansion $\phi_j(y) - \phi_j(x) = J_{\phi_j}(x)(y - x) + O(\|y - x\|^2)$. Only in the special case where $\phi_j(X_t) = Z_t$ holds (for instance, when ϕ_j is linear and the

feature-space path Z_t is induced by pushing forward the data-space path X_t , the optimal feature-space velocity can be written as

$$\begin{aligned} u_t^{z,*}(z) &\approx \mathbb{E}_{x \sim p_{x|z}} [J_{\phi_j}(x) u_t^{x,*}(x)] \\ u_{1-}^{z,*}(z) &\approx \mathbb{E}_{x \sim p_{x|z}} [J_{\phi_j}(x) u_{1-}^{x,*}(x)] \end{aligned} \quad (36)$$

see subsection A.5 for proof.

Note that, in general, we do not have $u_t^{z,*}(z) = \mathbb{E}_{x \sim p_{x|z}} [J_{\phi_j}(x) u_t^{x,*}(x)]$ and $u_{1-}^{z,*}(z) = \mathbb{E}_{x \sim p_{x|z}} [J_{\phi_j}(x) u_{1-}^{x,*}(x)]$. The discrepancy comes from the nonlinearity of ϕ_j (e.g., the encoder of MAE model). Nevertheless, deriving the feature-space Drifting objective in Equation 31 requires precisely the approximation $u_t^{z,*}(z) \approx \mathbb{E}_{x \sim p_{x|z}} [J_{\phi_j}(x) u_t^{x,*}(x)]$ and $u_{1-}^{z,*}(z) \approx \mathbb{E}_{x \sim p_{x|z}} [J_{\phi_j}(x) u_{1-}^{x,*}(x)]$. Under this assumption, taking the conditional expectation $\mathbb{E}_{x \sim p_{x|z}}$ on both sides of Equation 32, substituting Equation 36 and substituting the closed-form expressions of $u_t^{z,*}(z)$ and $u_{1-}^{z,*}(z)$, and letting $\Delta t \rightarrow 0$ yields

$$\begin{aligned} \mathcal{L}(\theta) &= \mathbb{E}_{x_0 \sim p_0} \mathbb{E}_{x^\theta \sim p_{x|z}(x^\theta | \phi_j(\psi_{0 \rightarrow 1}^\theta(x_0)))} \left[\|\phi_j(x^\theta) - \text{sg}(\phi_j(x^\theta)) + \frac{1}{2} \left(\frac{\mathbb{E}_{x_1 \sim p_1} [(\phi_j(x_1) - \phi_j(x^\theta)) k_1^\epsilon(\phi_j(x_1), \phi_j(x^\theta))]}{\mathbb{E}_{x_1 \sim p_1} [k_1^\epsilon(\phi_j(x_1), \phi_j(x^\theta))]} \right) \right. \\ &\quad \left. + \frac{\mathbb{E}_{x_1^\theta = \psi_{0 \rightarrow 1}^\theta(x_0'), x_0' \sim p_0} [(\phi_j(x_1^\theta) - \phi_j(x_1^\theta)) k_1^\epsilon(\phi_j(x_1^\theta), \phi_j(x_1^\theta))]}{\mathbb{E}_{x_1^\theta = \psi_{0 \rightarrow 1}^\theta(x_0'), x_0' \sim p_0} [k_1^\epsilon(\phi_j(x_1^\theta), \phi_j(x_1^\theta))]} \right] \end{aligned} \quad (37)$$

which recovers the feature-space Drifting Model loss in Equation 31.

The above derivation suggests the following two takeaways:

- 1. Dimensionality Considerations in Feature-Space Drifting.** Drifting in high-dimensional spaces \mathcal{X} faces the challenge of the curse of dimensionality, which motivates the model to operate in a feature space \mathcal{Z} . However, the direct objective defined in the feature space (see Equation 33) still evaluates kernels in the original space \mathcal{X} and, as a result, may not fully alleviate the associated high-dimensional effects.
- 2. Linearity Assumption for Feature-Space Velocity Approximation.** Evaluating kernels in feature space requires introducing Flow Matching directly in the feature domain. To make the corresponding feature-space closed-form velocity (Equation 36) compatible with the velocity term in Equation 32 (e.g., $J_{\phi_j}(x_{1-\Delta t}^\theta) u_{1-\Delta t}(x_{1-\Delta t}^\theta)$), the derivation typically adopts a linearity assumption on ϕ_j , leading to a simplified relationship between feature-space and data-space dynamics (e.g., $u_t^{z,*}(z) \approx \mathbb{E}_{x \sim p_{x|z}} [J_{\phi_j}(x) u_t^{x,*}(x)]$ in Equation 36). In practice, however, feature mappings ϕ_j are generally nonlinear (e.g., MAE encoders), and Deng et al. [2026] mitigates the impact of this approximation by enlarging the number of feature representations considered.

The reliance on a linearity assumption for ϕ_j also provides an intuitive explanation for why many features (often thousands) are used in practice Deng et al. [2026]: multiple feature maps jointly form a faithful surrogate direction for optimizing $\psi_{0 \rightarrow 1}^\theta$. Our experiments in subsection 6.2 further support this view, showing that using only a small number of features leads to weaker optimization performance even when the features are information-preserving.

This observation also leaves an open question:

Question 5.3. *How can we better design ϕ_j , or modify the feature-space objective, so that feature-space optimization more faithfully matches the original-space objective?*

6 Experiment

We conduct experiments in two settings. (1) 2D examples for likelihood learning: we validate our likelihood learning framework against analytically available ground truth. (2) Image generation: we implement the method on CelebA-HQ dataset, study the effects of learning rate and batch size, and verify the key claims of feature-space optimization. Implementation-wise, our derivation differs from Drifting Model primarily in the kernel choice; we further evaluate the flow-map-induced Gaussian kernel on CelebA-HQ and demonstrate its practicality.

6.1 2D Examples for Likelihood Learning

We consider three 2D point datasets, Spiral, Checkerboard, and Two Moons (Figure 4a), each with 50K samples. We learn the generative Long-Short Flow Map using Equation 17 with an 8-layer MLP of width 128; the resulting samples are shown in Figure 4b. To validate our likelihood learning formulation (Equation 27), we use the same MLP



Figure 3: Unconditional latent generation results on CelebA-HQ. We train for 100K steps using feature-space optimization with a pretrained MAE as the feature extractor and achieve an FID of 14.71. For comparison, the corresponding MeanFlow model reaches an FID of 12.4 after 400K training steps. Full results are provided in Table 1.

architecture and compare two training views, Eulerian and Lagrangian. In the Eulerian view, we set p_{sample} to a uniform distribution over the domain to learn the global density. In the Lagrangian view, we sample $p_{\text{sample}} = \psi_{t \rightarrow r}^\theta(x_0), x_0 \sim p_0$, where $\psi_{t \rightarrow r}^\theta$ is the learned flow map, focusing density learning around the data manifold. The Eulerian and Lagrangian results are reported in Figure 4c and Figure 4d. Overall, our Long-Short Flow-Map likelihood recovers the data distribution well. All runs use a batch size of 4096 and a learning rate of 10^{-4} . We train for 600K, 50K, and 150K steps on Spiral, Checkerboard, and Two Moons, respectively, and set ϵ to 0.5, 0.2, and 0.5 accordingly.

6.2 Image Generation

We evaluate the Long-Short Flow-Map method/Drifting Model on unconditional image generation using CelebA-HQ Karras et al. [2017], which contains 30,000 high-quality face images. Following Deng et al. [2026], we perform latent space generation with a DiT-B/2 backbone Peebles and Xie [2023] and a pretrained VAE from Stable Diffusion Rombach et al. [2022], and optimize the objective in feature space. Concretely, we extract latent features using a pretrained MAE encoder He et al. [2022]. Detailed architectures, hyperparameters, and training settings are provided in subsection B.1. We first sweep the learning rate and batch size as in subsection B.2.2 to study their impact on sample quality, and the results are shown in Figure 5a, 5b and 5c.

We further test the claim in section 5 that feature-space optimization is an imperfect proxy for the original objective, and therefore benefits from using many features to better recover the true update direction. To conduct this ablation study, we compare the default setting in Deng et al. [2026], which uses thousands of features, with a reduced setting that uses only four features obtained by taking the full feature maps from the four-stage MAE encoder outputs at different resolutions and treating each full feature map as a single feature. We also include a baseline without feature-space optimization, as shown in Figure 5f and Figure 7. Without feature-space optimization, training fails completely. Using only four features enables learning, but introduces visible distortions compared with using thousands of features, even though these four features collectively retain the full latent information.

Finally, our derivation of the Long-Short Flow-Map method differs from the original Drifting Model primarily in the kernel form. The Drifting Model adopts a Laplacian kernel $\exp(-\|y - x\|/\epsilon)$ for $k_t(\cdot, \cdot)$, whereas our flow-map derivation with the initial Gaussian noise yields a Gaussian kernel, $\exp(-\|y - x\|^2/\epsilon)$. As shown in Figure 5d and Figure 5e, the Gaussian kernel remains effective on CelebA-HQ and achieves results comparable to, and in some settings even better than, the original kernel. Moreover, Deng et al. [2026] reports ImageNet experiments with batch sizes of at least 4096, which raises concerns about the practical applicability of the Drifting Model. In contrast, we find that with appropriate learning-rate tuning, the long-short flow-map method/Drifting Model can still produce strong samples on CelebA-HQ with a standard batch size of 64 (see Figure 6), suggesting that the method may be more practical than previously implied.

7 Related Work

Flow Map Methods. Diffusion and flow matching models typically require many sampling steps, which motivates recent interest in one step or few step generation. Consistency Models Song et al. [2023], Song and Dhariwal [2023], Geng et al. [2025c], Lu and Song [2025] are an early representative that explicitly learns long range mappings by

enforcing consistency across time. The flow map viewpoint was later formalized in Boffi et al. [2025], where the core objective is to learn time indexed transport maps that satisfy trajectory consistency, also known as the semigroup property. Building on this perspective, a line of methods such as Shortcut Models Frans et al. [2025] and SplitMeanFlow Guo et al. [2025] progressively distill an instantaneous velocity field into long horizon mappings. In parallel, MeanFlow Geng et al. [2025a], α -Flow Zhang et al. [2025], and subsequent variants Li et al. [2025, 2026a], Geng et al. [2025b], Lu et al. [2026] learn via a continuity equation induced by the mean velocity defined by the flow map, providing an alternative route to train long distance transport without explicitly integrating many small steps. The long-short flow-map perspective was also proposed for the simulation of flow dynamics in physical space (e.g., Yin et al. [2021, 2023], Nave et al. [2010], Zhou et al. [2024], Deng et al. [2023]), where adaptive flow maps are used to reduce numerical dissipation in transport and fluid simulation. Prior work in this literature suggests that a single-scale flow map can be suboptimal, and that combining a long-range map for accumulated transport with a short-range map for local updates can better balance long-term fidelity and local accuracy (e.g., see Zhou et al. [2024]).

Closed-Form Different from prior work that mainly optimizes the Flow Matching regression objective, recent studies analyze the induced velocity field via the analytic closed-form solution Bertrand et al. [2025]. Since evaluating such velocities requires expensive kernel-weighted aggregation over the dataset, this line of work is used mostly for theory, including stability analysis Sprague et al. [2024], memorization and generalization Gao and Li [2024], Bertrand et al. [2025], Li et al. [2026b], and inference-time dynamics and acceleration Wan et al. [2024].

Distribution Moment Matching. Moment matching aligns model and data distributions by minimizing kernel discrepancies under the Maximum Mean Discrepancy (MMD) criterion Li et al. [2015], Dziugaite et al. [2015]. In GANs, this idea has been widely adopted, for example in MMD GANs and related variants Li et al. [2017], which match distribution moments using Gaussian or Laplace kernels. Closely related, Coulomb GAN Unterthiner et al. [2017] models learning via a Coulomb-style potential field and employs a Plummer-type kernel, which has been shown to lead to the optimal solution. Recently, moment matching has regained attention in one-step generation: inductive moment matching extends MMD-style objectives to one- or few-step diffusion by constructing positive and negative samples along the sampling path Zhou et al. [2025]. Drifting Model Deng et al. [2026] is also kernel-based, but instead formulates distribution alignment through a drifting field that measures the discrepancy between the current and target distributions and explicitly governs sample updates during training. Compared to standard MMD objectives, it provides a more flexible framework via a normalized kernel formulation, feature-space optimization, and extensions that support classifier-free guidance.

8 Conclusion

In this paper, we present the long-short flow-map perspective of the Drifting Model. This interpretation helps explain several of its key design choices. Building on this understanding, we derive a likelihood-based learning formulation and provide an in-depth discussion of feature-space optimization.

Several questions remain open. First, conditional generation with classifier-free guidance would benefit from a more principled formulation of CFG within this framework, together with systematic empirical evaluation. Second, the design of the feature-space encoder and the associated objective is not yet fully understood; in particular, it remains unclear how to construct feature representations that yield faithful optimization directions with fewer or more structured features. Looking ahead, this long-short flow-map perspective may extend beyond image generation to settings such as function generation and generation on manifolds. Finally, our analysis reveals an explicit connection between the noise distribution and the induced kernel form, suggesting a potential link between kernel design and recent noise optimization strategies Huang et al. [2024]. We expect that further exploration of this connection could motivate new methodological developments.

References

- Mingyang Deng, He Li, Tianhong Li, Yilun Du, and Kaiming He. Generative modeling via drifting. *arXiv preprint arXiv:2602.04770*, 2026.
- Yaron Lipman, Ricky T. Q. Chen, Heli Ben-Hamu, Maximilian Nickel, and Matt Le. Flow matching for generative modeling. In *International Conference on Learning Representations (ICLR)*, 2023.
- Yaron Lipman, Marton Havasi, Peter Holderrieth, Neta Shaul, Matt Le, Brian Karrer, Ricky TQ Chen, David Lopez-Paz, Heli Ben-Hamu, and Itai Gat. Flow matching guide and code. *arXiv preprint arXiv:2412.06264*, 2024.
- Kevin Frans, Danijar Hafner, Sergey Levine, and Pieter Abbeel. One step diffusion via shortcut models. In *International Conference on Learning Representations (ICLR)*, 2025.

- Zhengyang Geng, Mingyang Deng, Xingjian Bai, J Zico Kolter, and Kaiming He. Mean flows for one-step generative modeling. In *Neural Information Processing Systems (NeurIPS)*, 2025a.
- Zhengyang Geng, Yiyang Lu, Zongze Wu, Eli Shechtman, J Zico Kolter, and Kaiming He. Improved mean flows: On the challenges of fastforward generative models. *arXiv preprint arXiv:2512.02012*, 2025b.
- Yang Song, Prafulla Dhariwal, Mark Chen, and Ilya Sutskever. Consistency models. In *International Conference on Machine Learning (ICML)*, 2023.
- Linqi Zhou, Stefano Ermon, and Jiaming Song. Inductive moment matching. In *International Conference on Machine Learning (ICML)*, 2025.
- Quentin Bertrand, Anne Gagneux, Mathurin Massias, and Rémi Emonet. On the closed-form of flow matching: Generalization does not arise from target stochasticity. *arXiv preprint arXiv:2506.03719*, 2025.
- Yi Guo, Wei Wang, Zhihang Yuan, Rong Cao, Kuan Chen, Zhengyang Chen, Yuanyuan Huo, Yang Zhang, Yuping Wang, Shouda Liu, et al. Splitmeanflow: Interval splitting consistency in few-step generative modeling. *arXiv preprint arXiv:2507.16884*, 2025.
- Nicholas Matthew Boffi, Michael Samuel Albergo, and Eric Vanden-Eijnden. Flow map matching with stochastic interpolants: A mathematical framework for consistency models. *Transactions on Machine Learning Research (TMLR)*, 2025.
- Xingchang Huang, Corentin Salaun, Cristina Vasconcelos, Christian Theobalt, Cengiz Oztireli, and Gurprit Singh. Blue noise for diffusion models. In *ACM SIGGRAPH 2024 conference papers*, pages 1–11, 2024.
- Yujia Li, Kevin Swersky, and Rich Zemel. Generative moment matching networks. In *International conference on machine learning*, pages 1718–1727. PMLR, 2015.
- Gintare Karolina Dziugaite, Daniel M Roy, and Zoubin Ghahramani. Training generative neural networks via maximum mean discrepancy optimization. *arXiv preprint arXiv:1505.03906*, 2015.
- Xinyue Ai, Yutong He, Albert Gu, Ruslan Salakhutdinov, J Zico Kolter, Nicholas Matthew Boffi, and Max Simchowitz. Joint distillation for fast likelihood evaluation and sampling in flow-based models. *arXiv preprint arXiv:2512.02636*, 2025.
- Kaiming He, Xinlei Chen, Saining Xie, Yanghao Li, Piotr Dollár, and Ross Girshick. Masked autoencoders are scalable vision learners. In *Proceedings of the IEEE/CVF conference on computer vision and pattern recognition*, pages 16000–16009, 2022.
- Tero Karras, Timo Aila, Samuli Laine, and Jaakko Lehtinen. Progressive growing of gans for improved quality, stability, and variation. *arXiv preprint arXiv:1710.10196*, 2017.
- William Peebles and Saining Xie. Scalable diffusion models with transformers. In *IEEE Conference on Computer Vision and Pattern Recognition (CVPR)*, 2023.
- Robin Rombach, Andreas Blattmann, Dominik Lorenz, Patrick Esser, and Björn Ommer. High-resolution image synthesis with latent diffusion models. In *Proceedings of the IEEE/CVF conference on computer vision and pattern recognition*, pages 10684–10695, 2022.
- Yang Song and Prafulla Dhariwal. Improved techniques for training consistency models. In *International Conference on Learning Representations (ICLR)*, 2023.
- Zhengyang Geng, Ashwini Pokle, Weijian Luo, Justin Lin, and J Zico Kolter. Consistency models made easy. In *International Conference on Learning Representations (ICLR)*, 2025c.
- Cheng Lu and Yang Song. Simplifying, stabilizing and scaling continuous-time consistency models. In *International Conference on Learning Representations (ICLR)*, 2025.
- Huijie Zhang, Aliaksandr Siarohin, Willi Menapace, Michael Vasilkovsky, Sergey Tulyakov, Qing Qu, and Ivan Skorokhodov. Alphaflow: Understanding and improving meanflow models. *arXiv preprint arXiv:2510.20771*, 2025.
- Zhiqi Li, Yuchen Sun, Greg Turk, and Bo Zhu. Functional mean flow in hilbert space. *arXiv preprint arXiv:2511.12898*, 2025.
- Zhiqi Li, Yuchen Sun, Duowen Chen, Jinjin He, and Bo Zhu. Trajectory consistency for one-step generation on euler mean flows. *arXiv preprint arXiv:2602.02571*, 2026a.
- Yiyang Lu, Susie Lu, Qiao Sun, Hanhong Zhao, Zhicheng Jiang, Xianbang Wang, Tianhong Li, Zhengyang Geng, and Kaiming He. One-step latent-free image generation with pixel mean flows. *arXiv preprint arXiv:2601.22158*, 2026.
- Xi-Yuan Yin, Olivier Mercier, Badal Yadav, Kai Schneider, and Jean-Christophe Nave. A characteristic mapping method for the two-dimensional incompressible euler equations. *Journal of Computational Physics*, 424:109781, 2021.

- Xi-Yuan Yin, Kai Schneider, and Jean-Christophe Nave. A characteristic mapping method for the three-dimensional incompressible euler equations. *Journal of Computational Physics*, 477:111876, 2023.
- Jean-Christophe Nave, Rodolfo Ruben Rosales, and Benjamin Seibold. A gradient-augmented level set method with an optimally local, coherent advection scheme. *Journal of Computational Physics*, 229(10):3802–3827, 2010.
- Junwei Zhou, Duowen Chen, Molin Deng, Yitong Deng, Yuchen Sun, Sinan Wang, Shiyong Xiong, and Bo Zhu. Eulerian-lagrangian fluid simulation on particle flow maps. *ACM Transactions on Graphics (TOG)*, 43(4):1–20, 2024.
- Yitong Deng, Hong-Xing Yu, Diyang Zhang, Jiajun Wu, and Bo Zhu. Fluid simulation on neural flow maps. *ACM Transactions on Graphics (TOG)*, 42(6):1–21, 2023.
- Christopher Iliffe Sprague, Arne Elofsson, and Hossein Azizpour. Stable autonomous flow matching. *arXiv preprint arXiv:2402.05774*, 2024.
- Weiguo Gao and Ming Li. How do flow matching models memorize and generalize in sample data subspaces? *arXiv preprint arXiv:2410.23594*, 2024.
- Ziyun Li, Huancheng Hu, Soon Hoe Lim, Xuyu Li, Fei Gao, Enmao Diao, Zezhen Ding, Michalis Vazirgiannis, and Henrik Bostrom. A kinetic-energy perspective of flow matching. *arXiv preprint arXiv:2602.07928*, 2026b.
- Zhengchao Wan, Qingsong Wang, Gal Mishne, and Yusu Wang. Elucidating flow matching ode dynamics with respect to data geometries and denoisers. *arXiv preprint arXiv:2412.18730*, 2024.
- Chun-Liang Li, Wei-Cheng Chang, Yu Cheng, Yiming Yang, and Barnabás Póczos. Mmd gan: Towards deeper understanding of moment matching network. *Advances in neural information processing systems*, 30, 2017.
- Thomas Unterthiner, Bernhard Nessler, Calvin Seward, Günter Klambauer, Martin Heusel, Hubert Ramsauer, and Sepp Hochreiter. Coulomb gans: Provably optimal nash equilibria via potential fields. *arXiv preprint arXiv:1708.08819*, 2017.
- ZhMartin Heusel, Hubert Ramsauer, Thomas Unterthiner, Bernhard Nessler, and Sepp Hochreiter. Gans trained by a two time-scale update rule converge to a local nash equilibrium models. In *Neural Information Processing Systems (NeurIPS)*, 2017.
- Jonathan Ho and Tim Salimans. Classifier-free diffusion guidance. *arXiv preprint arXiv:2207.12598*, 2022.

A Missing Proofs and Theorems

A.1 Proof of Theorem 2.1

Theorem 2.1 Closed-Form Solution of Flow Matching Equation 3 admits an optimal solution

$$u_t^*(x) = \mathbb{E}_{x_1 \sim p_{1|t}(x_1|x)}[u_t(x|x_1)] = \frac{\mathbb{E}_{x_1 \sim p_{1|t}(x_1|x)}[x_1] - x}{1-t}, \quad (38)$$

which further admits a closed-form expression

$$u_t^*(x) = \frac{\mathbb{E}_{x_1 \sim p_1}[\frac{x_1-x}{1-t} k_t(x_1, x)]}{\mathbb{E}_{x_1 \sim p_1}[k_t(x_1, x)]}, \quad k_t(y, x) = e^{-\frac{\|ty-x\|^2}{2(1-t)^2}} \quad (39)$$

Proof. Because the objective in Equation 3 is an l_2 regression, the minimizer is given by the conditional expectation namely, $u_t^*(x) = \mathbb{E}[u_t(x|x_1)|x] = \mathbb{E}_{x_1 \sim p_{1|t}(x_1|x)}[u_t(x|x_1)]$. Because $u_t(x|x_1) = \frac{x_1-x}{1-t}$, we have $u_t^*(x) = \mathbb{E}_{x_1 \sim p_{1|t}(x_1|x)}[\frac{x_1-x}{1-t}] = \frac{\mathbb{E}_{x_1 \sim p_{1|t}(x_1|x)}[x_1] - x}{1-t}$.

Expanding the expectation $\mathbb{E}_{x_1 \sim p_{1|t}(x_1|x)}[\frac{x_1-x}{1-t}]$, we obtain

$$\begin{aligned} \mathbb{E}_{x_1 \sim p_{1|t}(x_1|x)}[\frac{x_1-x}{1-t}] &= \int \frac{x_1-x}{1-t} p_{1|t}(x_1|x) dx_1 \\ &= \int \frac{x_1-x}{1-t} \frac{p_{t|1}(x|x_1)p_1(x_1)}{\int p_{t|1}(x|x_1)p_1(x_1) dx} dx_1 \\ &= \frac{\int \frac{x_1-x}{1-t} p_{t|1}(x|x_1)p_1(x_1) dx_1}{\int p_{t|1}(x|x_1)p_1(x_1) dx} \end{aligned} \quad (40)$$

We next compute $\int p_{t|1}(x|x_1)p_1(x_1) dx_1$ and $\int \frac{x_1-x}{1-t} p_{t|1}(x|x_1)p_1(x_1) dx_1$. For $\int \frac{x_1-x}{1-t} p_{t|1}(x|x_1)p_1(x_1) dx_1$, we have

$$\begin{aligned} \int \frac{x_1-x}{1-t} p_{t|1}(x|x_1)p_1(x_1) dx &= \int \int \frac{x_1-x}{1-t} p_{t|1,0}(x|x_1, x_0) p_0(x_0) dx_0 p_1(x_1) dx \\ &= \int \int \frac{x_1-x}{1-t} \delta_{x=tx_1+(1-t)x_0} p_0(x_0) dx_0 p_1(x_1) dx \\ &= \int \int \frac{x_1-x}{1-t} \delta_{x=tx_1+(1-t)x_0} p_0(\frac{x-tx_1}{1-t}) dx_0 p_1(x_1) dx \\ &= \int \frac{x_1-x}{1-t} p_0(\frac{x-tx_1}{1-t}) p_1(x_1) dx \\ &= \int \frac{x_1-x}{1-t} \frac{1}{(2\pi)^{\frac{d}{2}}} e^{-\|\frac{x-tx_1}{1-t}\|^2} p_1(x_1) dx \\ &= \frac{1}{(2\pi)^{\frac{d}{2}}} \mathbb{E}_{x_1 \sim p_1}[\frac{x_1-x}{1-t} k_t(x_1, x)] \end{aligned} \quad (41)$$

Similarly, we have $\int p_{t|1}(x|x_1)p_1(x_1) dx = \frac{1}{(2\pi)^{\frac{d}{2}}} \mathbb{E}_{x_1 \sim p_1}[k_t(x_1, x)]$. Therefore, we obtain:

$$u_t^*(x) = \frac{\mathbb{E}_{x_1 \sim p_1}[\frac{x_1-x}{1-t} k_t(x_1, x)]}{\mathbb{E}_{x_1 \sim p_1}[k_t(x_1, x)]} \quad (42)$$

□

A.2 Non-Existence of Conditional Flow Maps

Theorem A.1 (Non-Existence of Conditional Flow Maps Li et al. [2026a]). *There exists no conditional flow maps $\psi_{t \rightarrow r}(x|x_1)$ that simultaneously (1) is consistent with the conditional velocity $u(x|x_1)$ under Equation 6, and (2) satisfies the consistency relation $\psi_{t \rightarrow r}(x) = \mathbb{E}_{x_1 \sim p_{1|t}(x_1|x)}[\psi_{t \rightarrow r}(x|x_1)]$ with marginal flow maps. As a result, a self-consistent conditional flow map does not exist.*

Proof. First, we denote the mappings $\psi_{t \rightarrow r}(x)$ obtained from (1) and (2) as $\psi_{t \rightarrow r}^{(1)}(x)$ and $\psi_{t \rightarrow r}^{(2)}(x)$, respectively. Specifically, $\psi_{t \rightarrow r}^{(1)}(x) = \psi_{0 \rightarrow r}(\psi_{0 \rightarrow t}^{-1}(x))$, and $\psi_{t \rightarrow r}^{(2)}(x) = \mathbb{E}_{x_1 \sim p_t(x_1|x)}[\psi_{t \rightarrow r}(x|x_1)]$. It suffices to show that $\psi_{t \rightarrow r}^{(1)}(x) \neq \psi_{t \rightarrow r}^{(2)}(x)$. To this end, it is sufficient to prove that $\frac{d}{dt}\psi_{t \rightarrow r}^{(1)}(x) \neq \frac{d}{dt}\psi_{t \rightarrow r}^{(2)}(x)$ at $t = 0$.

$$\begin{aligned}
\frac{d}{dr}\psi_{t \rightarrow r}^{(2)}(x) &= \frac{d}{dr} \int_{x_1} \psi_{t \rightarrow r}(x|x_1) p_{1|t}(x_1|x) dx_1 \\
&= \int_{x_1} \frac{d}{dr} \psi_{t \rightarrow r}(x|x_1) p_{1|t}(x_1|x) dx_1 \\
&= \int_{x_1} u_r(\psi_{t \rightarrow r}(x|x_1)|x_1) \frac{p_1(x_1) p_{t|1}(x|x_1)}{p_t(x)} dx_1 \\
&= \int_{x_1} u_r(\psi_{t \rightarrow r}(x|x_1)|x_1) p_1(x_1) dx_1 \\
&= \int_{x_1} (x_1 - x) p_1(x_1) dx_1 \\
&= \mathbb{E}_{x_1 \sim p_1(x_1)}[x_1] - x
\end{aligned} \tag{43}$$

Consequently, if $\psi_{t \rightarrow r}^{(1)}(x) = \psi_{t \rightarrow r}^{(2)}(x)$ we must have $\frac{d}{dr}\psi_{0 \rightarrow r}(x) = \mathbb{E}_{x_1 \sim p_1(x_1)}[x_1] - x$, $\psi_{0 \rightarrow r}(x) = (\mathbb{E}_{x_1 \sim p_1(x_1)}[x_1] - x)r + x$, which implies $p_1 = (\psi_{0 \rightarrow 1})_{\#} p_0 = \delta_{\mathbb{E}_{x_1 \sim p_1(x_1)}[x_1]}$, where δ denotes the Dirac distribution at a single point, which contradicts the actual setting $p_1 = p_{data}$. \square

A.3 Proof of Theorem 3.1

Theorem 3.1 Closed-Form Solution of the Endpoint Velocity For Flow Matching, under mild smoothness assumptions on the underlying distributions, the optimal velocity satisfies $\lim_{t \rightarrow 1^-} u_t^*(x) = x$. Consequently, the left-limit endpoint velocity $u_{1^-}^*(x) \triangleq \lim_{t \rightarrow 1^-} u_t^*(x)$ admits the closed form for any $t \in [0, 1)$

$$u_{1^-}^*(x) = \mathbb{E}_{x_t \sim p_{t|1}(x_t|x)} \left[\frac{x - x_t}{1 - t} \right] = \frac{\mathbb{E}_{x_t \sim p_t} \left[\frac{x - x_t}{1 - t} k_t(x, x_t) \right]}{\mathbb{E}_{x_t \sim p_t} [k_t(x, x_t)]} \tag{44}$$

Proof. In the derivations below, for convenience, we adopt the random-variable notation from Flow Matching and use the conditional path $X_t = tX_1 + (1 - t)X_0$, where $X_1 \sim p_1$, $X_0 \sim p_0$, and $X_t \sim p_t$ are the random variables induced by this conditional probability path. For sufficiently smooth distributions, the limit $\lim_{\epsilon \rightarrow 0^+} \mathbb{E}[X_0|X_{1-\epsilon} = x] = \mathbb{E}[X_0|X_1 = x]$ exists. Therefore,

$$\begin{aligned}
\lim_{t \rightarrow 1^-} u_t(x) &= \lim_{\epsilon \rightarrow 0^+} \frac{x - \mathbb{E}[X_0|X_{1-\epsilon} = x]}{1 - (1 - \epsilon)} \\
&= x - \mathbb{E}[X_0|X_1 = x] \\
&\stackrel{\textcircled{1}}{=} x - \mathbb{E}[X_0] \\
&= x,
\end{aligned} \tag{45}$$

where $\textcircled{1}$ uses the independence of X_0 and X_1 . We next show that $\mathbb{E}[X_t|X_1 = x] = tx$.

$$\begin{aligned}
\mathbb{E}[X_t|X_1 = x] &= \mathbb{E}[tX_1 + (1 - t)X_0|X_1 = x] \\
&= tx + (1 - t)\mathbb{E}[X_0|X_1 = x] \\
&= tx + (1 - t)\mathbb{E}[X_0] \\
&= tx
\end{aligned} \tag{46}$$

Consequently, the endpoint velocity admits the representation

$$\begin{aligned}
u_{1^-}(x) &= \lim_{t \rightarrow 1} u_t(x) \\
&= x \\
&= \frac{x - \mathbb{E}[X_t|X_1 = x]}{1 - t} \\
&= \mathbb{E}_{x_t \sim p_{t|1}(x_t|x)} \left[\frac{x - x_t}{1 - t} \right]
\end{aligned} \tag{47}$$

Similar to subsection A.1, we now derive a closed-form expression for $u_1(x)$:

$$\begin{aligned}
 u_{1-}(x) &= \mathbb{E}_{x_t \sim p_{t|1}(x_t|x)} \left[\frac{x - x_t}{1-t} \right] \\
 &= \int \frac{x - x_t}{1-t} p_{t|1}(x_t|x) dx_t \\
 &= \int \frac{x - x_t}{1-t} \frac{p_{1|t}(x|x_t) p_t(x_t)}{\int_{x_t} p_{1|t}(x|x_t) p_t(x_t) dx_t} dx_t \\
 &= \frac{\int \frac{x-x_t}{1-t} p_{1|t}(x|x_t) p_t(x_t) dx_t}{\int p_{1|t}(x|x_t) p_t(x_t) dx_t}
 \end{aligned} \tag{48}$$

Next, we compute $\int p_{1|t}(x|x_t) p_t(x_t) dx_t$ and $\int \frac{x-x_t}{1-t} p_{1|t}(x|x_t) p_t(x_t) dx_t$. For $\int \frac{x-x_t}{1-t} p_{1|t}(x|x_t) p_t(x_t) dx_t$, we have

$$\begin{aligned}
 \int \frac{x - x_t}{1-t} p_{1|t}(x|x_t) p_t(x_t) dx_t &= \int_{x_t} \int_{x_0} \frac{x - x_t}{1-t} p_{1|t,0}(x|x_t, x_0) p_0(x_0) dx_0 p_t(x_t) dx_t \\
 &= \int \frac{x - x_t}{1-t} \int \delta(x = \frac{x_t - (1-t)x_0}{t}) \frac{1}{(2\pi)^{\frac{d}{2}}} e^{-\frac{1}{2}x_0^2} dx_0 p_t(x_t) dx_t \\
 &= \int \frac{x - x_t}{1-t} \frac{1}{(2\pi)^{\frac{d}{2}}} e^{-\frac{1}{2} \|\frac{x_t - tx}{1-t}\|^2} p_t(x_t) dx_t
 \end{aligned} \tag{49}$$

Similarly, we have $\int p(x|x_t) p_t(x_t) dx_t = \int \frac{1}{(2\pi)^{\frac{d}{2}}} e^{-\frac{1}{2} \|\frac{x_t - tx}{1-t}\|^2} p(x_t) dx_t$. Therefore, we have

$$u_{1-}(x) = \frac{\mathbb{E}_{x_t \sim p_t} \left[\frac{x-x_t}{1-t} k_t(x, x_t) \right]}{\mathbb{E}_{x_t \sim p_t} [k_t(x, x_t)]} \tag{50}$$

□

A.4 Proof of Theorem 4.1

Theorem 4.1 Closed-Form Solution for Velocity Divergence For the closed-form solution of the velocity field $u_t^*(x)$ in Equation 5 and the endpoint velocity $u_{1-}^*(x)$ in Equation 15 with the mollified kernel k_t^ϵ in Equation 11, their divergences can be also computed in closed form as

$$\begin{aligned}
 \nabla \cdot u_t^*(x) &= \frac{1}{1-t} \left[\frac{2t}{2(1-t)^2 + \epsilon} \left(\frac{\mathbb{E}_{x_1 \sim p_1} [\|x_1\|^2 k_t^\epsilon(x_1, x)]}{\mathbb{E}_{x_1 \sim p_1} [k_t^\epsilon(x_1, x)]} \right. \right. \\
 &\quad \left. \left. - \left\| \frac{\mathbb{E}_{x_1 \sim p_1} [x_1 k_t^\epsilon(x_1, x)]}{\mathbb{E}_{x_1 \sim p_1} [k_t^\epsilon(x_1, x)]} \right\|^2 \right) - d \right] \\
 \nabla \cdot u_{1-}^*(x) &= \frac{1}{1-t} \left[d - \frac{2t^2}{2(1-t)^2 + \epsilon} \left(\frac{\mathbb{E}_{x_t \sim p_t} [\|x_t\|^2 k_t^\epsilon(x, x_t)]}{\mathbb{E}_{x_t \sim p_t} [k_t^\epsilon(x, x_t)]} \right. \right. \\
 &\quad \left. \left. - \left\| \frac{\mathbb{E}_{x_t \sim p_t} [x_t k_t^\epsilon(x, x_t)]}{\mathbb{E}_{x_t \sim p_t} [k_t^\epsilon(x, x_t)]} \right\|^2 \right) \right]
 \end{aligned} \tag{51}$$

Proof. First, we compute the partial derivative of $k_t^\epsilon(y, x)$:

$$\begin{aligned}
 \frac{\partial k_t^\epsilon(y, x)}{\partial y} &= -\frac{2t(ty - x)}{2(1-t)^2 + \epsilon} e^{-\frac{\|ty - x\|^2}{2(1-t)^2 + \epsilon}} \\
 \frac{\partial k_t^\epsilon(y, x)}{\partial x} &= \frac{2(ty - x)}{2(1-t)^2 + \epsilon} e^{-\frac{\|ty - x\|^2}{2(1-t)^2 + \epsilon}}
 \end{aligned} \tag{52}$$

Then, we calculate $\nabla \cdot u_t^*(x)$ and $\nabla \cdot u_1^*(x)$, respectively. For $\nabla \cdot u_t^*(x)$, we have

$$\begin{aligned}
 & \nabla \cdot u_t^*(x) \\
 &= \nabla \cdot \left(\frac{\mathbb{E}_{x_1 \sim p_1} \left[\frac{x_1 - x}{1-t} k_t^\epsilon(x_1, x) \right]}{\mathbb{E}_{x_1 \sim p_1} [k_t^\epsilon(x_1, x)]} \right) \\
 &= \frac{\nabla \cdot \left(\frac{\mathbb{E}_{x_1 \sim p_1} [x_1 k_t^\epsilon(x_1, x)]}{\mathbb{E}_{x_1 \sim p_1} [k_t^\epsilon(x_1, x)]} \right) - d}{1-t} \\
 &= \frac{1}{1-t} \left[\frac{\nabla \cdot (\mathbb{E}_{x_1 \sim p_1} [x_1 k_t^\epsilon(x_1, x)]) \mathbb{E}_{x_1 \sim p_1} [k_t^\epsilon(x_1, x)] - \mathbb{E}_{x_1 \sim p_1} [x_1 k_t^\epsilon(x_1, x)] \cdot \nabla (\mathbb{E}_{x_1 \sim p_1} [k_t^\epsilon(x_1, x)])}{(\mathbb{E}_{x_1 \sim p_1} [k_t^\epsilon(x_1, x)])^2} - d \right] \\
 &= \frac{1}{1-t} \left[\frac{\mathbb{E}_{x_1 \sim p_1} [x_1 \cdot \nabla k_t^\epsilon(x_1, x)] \mathbb{E}_{x_1 \sim p_1} [k_t^\epsilon(x_1, x)] - \mathbb{E}_{x_1 \sim p_1} [x_1 k_t^\epsilon(x_1, x)] \cdot \mathbb{E}_{x_1 \sim p_1} [\nabla k_t^\epsilon(x_1, x)]}{(\mathbb{E}_{x_1 \sim p_1} [k_t^\epsilon(x_1, x)])^2} - d \right] \\
 &= \frac{1}{1-t} \left[\frac{\mathbb{E}_{x_1 \sim p_1} [x_1 \cdot \frac{2(tx_1 - x)}{2(1-t)^2 + \epsilon} k_t^\epsilon(x_1, x)] \mathbb{E}_{x_1 \sim p_1} [k_t^\epsilon(x_1, x)] - \mathbb{E}_{x_1 \sim p_1} [x_1 k_t^\epsilon(x_1, x)] \cdot \mathbb{E}_{x_1 \sim p_1} [\frac{2(tx_1 - x)}{2(1-t)^2 + \epsilon} k_t^\epsilon(x_1, x)]}{(\mathbb{E}_{x_1 \sim p_1} [k_t^\epsilon(x_1, x)])^2} - d \right] \\
 &= \frac{1}{1-t} \left[\frac{2t}{2(1-t)^2 + \epsilon} \frac{\mathbb{E}_{x_1 \sim p_1} [x_1 \cdot x_1 k_t^\epsilon(x_1, x)] \mathbb{E}_{x_1 \sim p_1} [k_t^\epsilon(x_1, x)] - \mathbb{E}_{x_1 \sim p_1} [x_1 k_t^\epsilon(x_1, x)] \cdot \mathbb{E}_{x_1 \sim p_1} [x_1 k_t^\epsilon(x_1, x)]}{(\mathbb{E}_{x_1 \sim p_1} [k_t^\epsilon(x_1, x)])^2} - d \right] \\
 &= \frac{1}{1-t} \left[\frac{2t}{2(1-t)^2 + \epsilon} \left(\frac{\mathbb{E}_{x_1 \sim p_1} [\|x_1\|^2 k_t^\epsilon(x_1, x)]}{\mathbb{E}_{x_1 \sim p_1} [k_t^\epsilon(x_1, x)]} - \left\| \frac{\mathbb{E}_{x_1 \sim p_1} [x_1 k_t^\epsilon(x_1, x)]}{\mathbb{E}_{x_1 \sim p_1} [k_t^\epsilon(x_1, x)]} \right\|^2 \right) - d \right]
 \end{aligned} \tag{53}$$

For $\nabla \cdot u_{1-}^*(x)$, we have

$$\begin{aligned}
 & \nabla \cdot u_{1-}^*(x) \\
 &= \nabla \cdot \left(\frac{\mathbb{E}_{x_t \sim p_t} \left[\frac{x - x_t}{1-t} k_t^\epsilon(x, x_t) \right]}{\mathbb{E}_{x_t \sim p_t} [k_t^\epsilon(x, x_t)]} \right) \\
 &= \frac{1}{1-t} \left[d - \frac{\nabla \cdot (\mathbb{E}_{x_t \sim p_t} [x_t k_t^\epsilon(x, x_t)]) \mathbb{E}_{x_t \sim p_t} [k_t^\epsilon(x, x_t)] - \mathbb{E}_{x_t \sim p_t} [x_t k_t^\epsilon(x, x_t)] \cdot \nabla (\mathbb{E}_{x_t \sim p_t} [k_t^\epsilon(x, x_t)])}{(\mathbb{E}_{x_t \sim p_t} [k_t^\epsilon(x, x_t)])^2} \right] \\
 &= \frac{1}{1-t} \left[d - \frac{\mathbb{E}_{x_t \sim p_t} [x_t \cdot \nabla k_t^\epsilon(x, x_t)] \mathbb{E}_{x_t \sim p_t} [k_t^\epsilon(x, x_t)] - \mathbb{E}_{x_t \sim p_t} [x_t k_t^\epsilon(x, x_t)] \cdot (\mathbb{E}_{x_t \sim p_t} [\nabla k_t^\epsilon(x, x_t)])}{(\mathbb{E}_{x_t \sim p_t} [k_t^\epsilon(x, x_t)])^2} \right] \\
 &= \frac{1}{1-t} \left[d - \frac{\mathbb{E}_{x_t \sim p_t} [x_t \cdot \frac{2(tx - x_t)}{2(1-t)^2 + \epsilon} k_t^\epsilon(x, x_t)] \mathbb{E}_{x_t \sim p_t} [k_t^\epsilon(x, x_t)] - \mathbb{E}_{x_t \sim p_t} [x_t k_t^\epsilon(x, x_t)] \cdot (\mathbb{E}_{x_t \sim p_t} [\frac{2(tx - x_t)}{2(1-t)^2 + \epsilon} k_t^\epsilon(x, x_t)])}{(\mathbb{E}_{x_t \sim p_t} [k_t^\epsilon(x, x_t)])^2} \right] \\
 &= \frac{1}{1-t} \left[d - \frac{\mathbb{E}_{x_t \sim p_t} [x_t \cdot \frac{-2t(tx - x_t)}{2(1-t)^2 + \epsilon} k_t^\epsilon(x, x_t)] \mathbb{E}_{x_t \sim p_t} [k_t^\epsilon(x, x_t)] - \mathbb{E}_{x_t \sim p_t} [x_t k_t^\epsilon(x, x_t)] \cdot (\mathbb{E}_{x_t \sim p_t} [\frac{-2t(tx - x_t)}{2(1-t)^2 + \epsilon} k_t^\epsilon(x, x_t)])}{(\mathbb{E}_{x_t \sim p_t} [k_t^\epsilon(x, x_t)])^2} \right] \\
 &= \frac{1}{1-t} \left[d - \frac{2t^2}{2(1-t)^2 + \epsilon} \left(\frac{\mathbb{E}_{x_t \sim p_t} [\|x_t\|^2 k_t^\epsilon(x, x_t)]}{\mathbb{E}_{x_t \sim p_t} [k_t^\epsilon(x, x_t)]} - \left\| \frac{\mathbb{E}_{x_t \sim p_t} [x_t k_t^\epsilon(x, x_t)]}{\mathbb{E}_{x_t \sim p_t} [k_t^\epsilon(x, x_t)]} \right\|^2 \right) \right]
 \end{aligned} \tag{54}$$

□

A.5 Proof of Theorem 5.2

Theorem 5.2 Feature-Data Space Optimal Velocity Relation Let $X_1 \sim p_1$ and define $Z_1 = \phi_j(X_1)$. Denote by $u_t^{z,*}(x)$ the optimal Flow Matching velocity in data space associated with the conditional path $X_t = tX_1 + (1-t)X_0$, and by $u_t^{z,*}(z)$ the optimal velocity in feature space associated with $Z_t = tZ_1 + (1-t)Z_0$, where X_0 and Z_0 are Gaussian reference variables on \mathcal{X} and \mathcal{Z} , respectively. We define $p_{x|z}(x|z)$ as the conditional distribution induced by the inverse of the deterministic map $z = \phi_j(x)$. Then, for $z = \phi_j(x)$, the two velocities satisfy the following approximate relations:

$$\begin{aligned}
 u_t^{z,*}(z) &\approx J_{\phi_j}(x) \frac{\mathbb{E}[X_1 | Z_t = \phi_j(x)] - x}{1-t}, \\
 u_{1-}^{z,*}(z) &\approx J_{\phi_j}(x) \frac{x - \mathbb{E}[X'_t | Z_1 = \phi_j(x)]}{1-t},
 \end{aligned} \tag{55}$$

where $J_{\phi_j}(x) = \frac{\partial \phi_j(x)}{\partial x}$ is the Jacobian of ϕ_j , and X'_t is an auxiliary \mathcal{X} -valued random variable satisfying $\phi_j(X'_t) = Z_t$ almost surely. The approximation \approx above follows from the first-order Taylor expansion $\phi_j(y) - \phi_j(x) = J_{\phi_j}(x)(y -$

$x) + O(\|y - x\|^2)$. Only in the special case where $\phi_j(X_t) = Z_t$ holds (for instance, when ϕ_j is linear and the feature-space path Z_t is induced by pushing forward the data-space path X_t), the optimal feature-space velocity can be written as

$$\begin{aligned} u_t^{z,*}(z) &\approx \mathbb{E}_{x \sim p_{x|z}} [J_{\phi_j}(x) u_t^{x,*}(x)] \\ u_{1-}^{z,*}(z) &\approx \mathbb{E}_{x \sim p_{x|z}} [J_{\phi_j}(x) u_{1-}^{x,*}(x)] \end{aligned} \quad (56)$$

Proof. Let $z = \phi_j(x)$. The optimal velocity $u_t^{z,*}(z)$ can be computed with first-order approximation:

$$\begin{aligned} u_t^{z,*}(z) &= \frac{\mathbb{E}[Z_1 - z | Z_t = z]}{1 - t} \\ &\stackrel{\textcircled{1}}{=} \frac{\mathbb{E}[\phi_j(X_1) - \phi_j(x) | Z_t = z]}{1 - t} \\ &\approx \frac{\mathbb{E}[J_{\phi_j}(x)(X_1 - x) | Z_t = z]}{1 - t} \\ &= \frac{J_{\phi_j}(x)(\mathbb{E}[X_1 | Z_t = z] - x)}{1 - t} \end{aligned} \quad (57)$$

where $\textcircled{1}$ holds because

$$\begin{aligned} \mathbb{E}[Z_1 | Z_t = z] &= \int z_1 p_{Z_1 | Z_t}(z_1 | z) dz_1 \\ &= \int \int \phi(x_1) p_{x|z}(x_1 | z_1) dx_1 p_{Z_1 | Z_t}(z_1 | z) dz_1 \\ &= \int \phi(x_1) \int p_{x|z}(x_1 | z_1) p_{Z_1 | Z_t}(z_1 | z) dz_1 dx_1 \\ &= \int \phi(x_1) \int p_{X_1 | Z_1, Z_t}(x_1 | z_1, z) p_{Z_1 | Z_t}(z_1 | z) dz_1 dx_1 \\ &= \int \phi(x_1) p_{X_1 | Z_t}(x_1 | z) dx_1 \\ &= \mathbb{E}[\phi_j(X_1) | Z_t = z] \end{aligned} \quad (58)$$

When $\phi_j(X_t) = Z_t$ holds, we have

$$\begin{aligned} u_t^{z,*}(z) &= \int \frac{z_1 - z}{1 - t} p_{Z_1 | Z_t}(z_1 | z) dz_1 \\ &= \int \frac{z_1 - z}{1 - t} \int p_{Z_1 | Z_t, X_t}(z_1 | z, x) p_{x|z}(x | z) dx dz_1 \\ &\stackrel{Z_t = \phi_j(X_t)}{=} \int \int \frac{z_1 - \phi_j(x)}{1 - t} p_{Z_1 | X_t}(z_1 | x) p_{x|z}(x | z) dx dz_1 \\ &= \int \frac{\int z_1 p_{Z_1 | X_t}(z_1 | x) dz_1 - \phi_j(x)}{1 - t} p_{x|z}(x | z) dx \\ &\stackrel{\textcircled{1}}{=} \int \frac{\int \phi_j(x_1) p_{X_1 | X_t}(x_1 | x) dx_1 - \phi_j(x)}{1 - t} p_{x|z}(x | z) dx \\ &= \int \int \frac{\phi_j(x_1) - \phi_j(x)}{1 - t} p_{X_1 | X_t}(x_1 | x) dx_1 p_{x|z}(x | z) dx \\ &\approx \int \int J_{\phi_j}(x) \frac{x_1 - x}{1 - t} p_{X_1 | X_t}(x_1 | x) dx_1 p_{x|z}(x | z) dx \\ &= \int J_{\phi_j}(x) u_t^{x,*}(x) p_{x|z}(x | z) dx \\ &= \mathbb{E}_{x \sim p_{x|z}} [J_{\phi_j}(x) u_t^{x,*}(x)] \end{aligned} \quad (59)$$

where ① holds because

$$\begin{aligned}
 \int z_1 p_{Z_1|X_t}(z_1|x) dz_1 &= \int \int \phi_j(x_1) p_{Z_1|X_t, X_1}(z_1|x, x_1) p_{X_1|X_t}(x_1|x) dx_1 dz_1 \\
 &= \int \int \phi_j(x_1) \delta_{z_1=\phi_j(x_1)} p_{X_1|X_t}(x_1|x) dx_1 dz_1 \\
 &= \int \phi_j(x_1) \int \delta_{z_1=\phi_j(x_1)} dz_1 p_{X_1|X_t}(x_1|x) dx_1 \\
 &= \int \phi_j(x_1) p_{X_1|X_t}(x_1|x) dx_1
 \end{aligned} \tag{60}$$

For $u_1^{z,*}(z)$, when there exists an auxiliary random variable X'_t such that $\phi_j(X'_t) = Z_t$ almost surely, we have

$$\begin{aligned}
 u_1^{z,*}(z) &= \frac{\mathbb{E}[z - Z_t | Z_1 = z]}{1 - t} \\
 &\stackrel{\text{①}}{=} \frac{\mathbb{E}[\phi_j(x) - \phi_j(X'_t) | Z_1 = z]}{1 - t} \\
 &\approx \frac{\mathbb{E}[J_{\phi_j}(x - X'_t) | Z_1 = z]}{1 - t} \\
 &= J_{\phi_j}(x) \frac{x - \mathbb{E}[X'_t | Z_1 = \phi_j(x)]}{1 - t}
 \end{aligned} \tag{61}$$

where ① holds because

$$\begin{aligned}
 \mathbb{E}[Z_t | Z_1 = z] &= \int z_t p_{Z_t|Z_1}(z_t|z) dz_t \\
 &= \int \int \phi_j(x'_t) p_{X'_t|Z_t}(x'_t|z_t) dx'_t p_{Z_t|Z_1}(z_t|z) dz_t \\
 &= \int \phi_j(x'_t) \left(\int p_{X'_t|Z_t}(x'_t|z_t) p_{Z_t|Z_1}(z_t|z) dz_t \right) dx'_t \\
 &= \int \phi_j(x'_t) \left(\int p_{X'_t|Z_t, Z_1}(x'_t|z_t, z) p_{Z_t|Z_1}(z_t|z) dz_t \right) dx'_t \\
 &= \int \phi_j(x'_t) p_{X'_t|Z_1}(x'_t|z) dx'_t \\
 &= \mathbb{E}[\phi_j(X'_t) | Z_1 = z]
 \end{aligned} \tag{62}$$

When $\phi_j(X_t) = Z_t$, X_t can be used as the X'_t , namely $\phi_j(X_t) = Z_t$.

$$\begin{aligned}
u_1^{z,*}(z) &= \int \frac{z - z_t}{1 - t} p_{Z_t|Z_1}(z_t|z) dz_t \\
&= \int \frac{z - z_t}{1 - t} \int p_{Z_t|Z_1, X_1}(z_t|z, x) p_{x|z}(x|z) dx dz_t \\
&= \int \int \frac{\phi_j(x) - z_t}{1 - t} p_{Z_t|X_1}(z_t|x) p_{x|z}(x|z) dx dz_t \\
&= \int \frac{\phi_j(x) - \int z_t p_{Z_t|X_1}(z_t|x) dz_t}{1 - t} p_{x|z}(x|z) dx \\
&\stackrel{\textcircled{1}}{=} \int \frac{\phi_j(x) - \int \phi_j(x_t) p_{X_t|X_1}(x_t|x) dx_t}{1 - t} p_{x|z}(x|z) dx \\
&= \int \int \frac{\phi_j(x) - \phi_j(x_t)}{1 - t} p_{x|z}(x|z) p_{X_t|X_1}(x_t|x) dx_t dx \\
&\approx \int \int J_{\phi_j}(x) \frac{x - x_t}{1 - t} p_{x|z}(x|z) p_{X_t|X_1}(x_t|x) dx_t dx \\
&= \int J_{\phi_j}(x) \int \frac{x - x_t}{1 - t} p_{X_t|X_1}(x_t|x) dx_t p_{x|z}(x|z) dx \\
&= \int J_{\phi_j}(x) u_1^{x,*}(x) p_{x|z}(x|z) dx \\
&= \mathbb{E}_{x \sim p_{x|z}} [J_{\phi_j}(x) u_1^{x,*}(x)]
\end{aligned} \tag{63}$$

where $\textcircled{1}$ holds because

$$\begin{aligned}
\int z_t p_{Z_t|X_1}(z_t|x) dz_t &= \int \int \phi_j(x_t) p_{Z_t|X_1, X_t}(z_t|x, x_t) p_{X_t|X_1}(x_t|x) dx_t dz_t \\
&\stackrel{Z_t = \phi_j(X_t)}{=} \int \int \phi_j(x_t) \delta_{z_t = \phi_j(x_t)} p_{X_t|X_1}(x_t|x) dx_t dz_t \\
&= \int \phi_j(x_t) \int \delta_{z_t = \phi_j(x_t)} dz_t p_{X_t|X_1}(x_t|x) dx_t \\
&= \int \phi_j(x_t) p_{X_t|X_1}(x_t|x) dx_t
\end{aligned} \tag{64}$$

□

B Training and Results

B.1 Training Details

For the image generation task, we use DiT-B/2 as the backbone. Unless otherwise specified, we train with batch sizes in $\{64, 256, 1024\}$, for 100K steps, using EMA with decay 0.9999 and Adam with $(\beta_1, \beta_2) = (0.9, 0.95)$. We consider learning rates in $\{2.5 \times 10^{-5}, 5 \times 10^{-5}, 1 \times 10^{-4}, 2 \times 10^{-4}\}$ and weight decay 0, with a 5K-step learning-rate warmup. Unless otherwise specified, we use a constant learning-rate schedule. For the experiment in Figure 6, we focus on improving generation quality under the small batch size (64) setting by training for 400K steps with a staged schedule: 5×10^{-5} for steps 0-200K, 2.5×10^{-5} for steps 200K-300K, and 1.25×10^{-5} for steps 300K-400K. We use FP16 mixed precision for the main model computation, while computing the kernel k_1^ϵ in Equation 13 and Equation 17 in FP32.

We use the pretrained VAE `sd-vae-ft-mse` from Rombach et al. [2022]. For the MAE encoder, we follow the ResNet-based architecture in Deng et al. [2026] with four resolutions $(32^2, 16^2, 8^2, 4^2)$ and a base width of 256. We train the MAE for 250K steps with EMA decay 0.9995 and Adam with $(\beta_1, \beta_2) = (0.9, 0.999)$, using a learning rate of 5×10^{-4} without warmup. We mask 2×2 patches by zeroing, where each patch is independently masked with probability 0.5. When extracting MAE features, we use all feature types (a-d) from Section A.5 of Deng et al. [2026], and combine computations under three temperatures (0.02, 0.05, and 0.2) within the same feature space. Moreover, instead of taking features every two blocks, we take the output features at each resolution, resulting in several thousand feature channels in total.

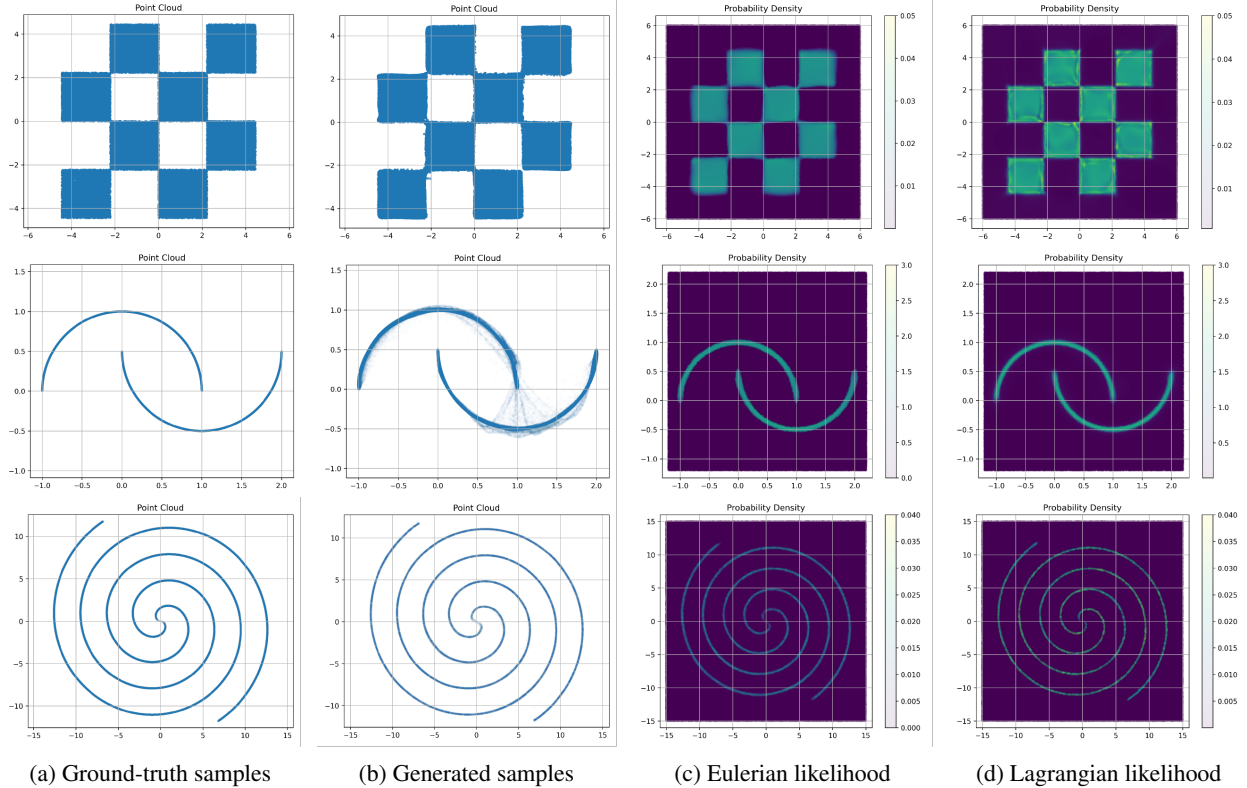


Figure 4: **2D Examples.** We show the ground-truth samples, generated samples, and learned likelihoods from the Eulerian and Lagrangian views on Spiral, Checkerboard, and Two Moons.

B.2 Results

B.2.1 2D Examples for Likelihood Learning

In Figure 4, we present the ground-truth distributions, generated samples, and the learned likelihoods under both the Eulerian and Lagrangian views for the Spiral, Checkerboard, and Two Moons datasets.

B.2.2 Image Generation

In Figure 5a, 5b, 5c, 5d and 5e, we evaluate the Long-Short Flow-Map method/the Drifting Model under various learning rates and batch sizes, reporting results at 100K training steps. We consider both the Laplacian kernel used in the original Drifting Model and the Gaussian kernel derived in our analysis, and compute FID Heusel et al. [2017] by generating 50K images. In Figure 5f and Figure 7, we conduct ablation studies on feature-space optimization. Specifically, Figure 5f reports the quantitative results, while Figure 7 provides a qualitative comparison of optimization in the default feature setting used in Deng et al. [2026] (with thousands of feature channels), a reduced feature setting with only a few features, and the original space. In Figure 6, we show results from the Long-Short Flow-Map method/Drifting Model trained for 400K iterations with batch size 64 (with tuned learning rate), demonstrating that strong sample quality is achievable without extremely large batch sizes. Finally, in Table 1, we compare our method against other one-step generative baselines.

C Discussion on Classifier-Free Guidance

Since our computation of the short flow-map segment $\psi_{1-\Delta t \rightarrow 1}$ is essentially based on numerically integrating the velocity field, and the velocity is obtained from the closed-form solution in flow matching, it is natural to incorporate CFG when evaluating the velocity on this short segment. Below we outline some possible choices, and exploring a broader design space together with empirical validation is left for future work.

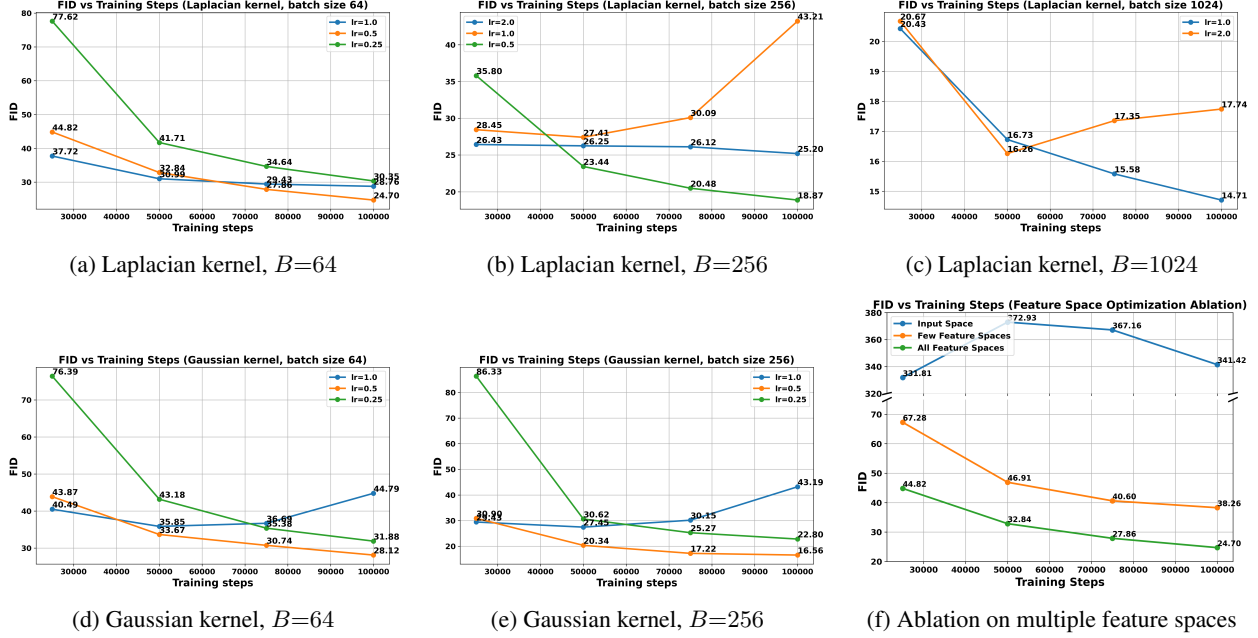


Figure 5: **Image generation.** FID trajectories under different kernels and batch sizes, together with an ablation on using multiple feature spaces. The Laplacian kernel corresponds to the first-order kernel used in Drifting Model Deng et al. [2026], whereas the Gaussian kernel is the second-order kernel derived in our framework. Overall, the Gaussian kernel performs comparably to the Laplacian kernel, and can be better in some regimes. In the ablation (batch size $B=64$, $lr=5 \times 10^{-5}$), we compare using the default feature set with thousands of channels, using only four features (the outputs at the four encoder resolutions), and operating directly in the original space; The latter two settings fail to produce high-quality results.

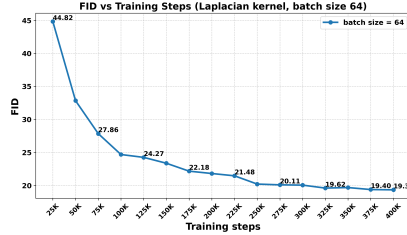


Figure 6: **FID over training with a standard batch size.** FID curves for the Long-Short Flow-Map method / Drifting Model over training, using batch size 64 (with a tuned learning rate). The results show that strong generative performance can be achieved without extremely large batch sizes.

1. **CFG on the velocity field u_t .** In Equation 9 and Equation 14, estimating $\psi_{1-\Delta t \rightarrow 1}$ introduces the velocity $u_{1-\Delta t}$. With CFG, we can replace the conditional velocity by $u_{1-\Delta t}(x|y) \leftarrow w u_{1-\Delta t}(x|y) + (1-w) u_{1-\Delta t}(x|\emptyset)$, where y denotes the class label, \emptyset denotes the null condition, and w is the guidance scale. In the limiting case, this modification turns the $\frac{\mathbb{E}_{x_1 \sim p_1} [(x_1 - \psi_{0 \rightarrow 1}^\theta(x_0)) k_1(x_1, \psi_{0 \rightarrow 1}^\theta(x_0))]}{\mathbb{E}_{x_1 \sim p_1} [k_1(x_1, \psi_{0 \rightarrow 1}^\theta(x_0))]}$ term in Equation 13 and Equation 17 into $w \frac{\mathbb{E}_{x_1 \sim p_1} [(x_1 - \psi_{0 \rightarrow 1}^\theta(x_0|y)) k_1(x_1, \psi_{0 \rightarrow 1}^\theta(x_0|y))]}{\mathbb{E}_{x_1 \sim p_1} [k_1(x_1, \psi_{0 \rightarrow 1}^\theta(x_0|y))]} + (1-w) \frac{\mathbb{E}_{x_1 \sim p_1} [(x_1 - \psi_{0 \rightarrow 1}^\theta(x_0|\emptyset)) k_1(x_1, \psi_{0 \rightarrow 1}^\theta(x_0|\emptyset))]}{\mathbb{E}_{x_1 \sim p_1} [k_1(x_1, \psi_{0 \rightarrow 1}^\theta(x_0|\emptyset))]}$.
2. **CFG on the target distribution p_1 .** Beyond modifying the velocity field, CFG can also be interpreted as modifying the underlying target distribution Ho and Salimans [2022]. Concretely, one may replace $p_1(x|y)$ by its CFG-guided counterpart $p_1^{\text{cfg}} = p_1^w(x|y) p_1^{1-w}(x|\emptyset)$, which correspond-

Table 1: **Comparison under different training budgets.** We report the batch size, training steps, and FID for our method and prior baselines using a DiT-B/2 backbone for one-step latent-space generation.

Method	Batch size	Training steps	FID
Consistency Models Song et al. [2023]	64	400K	33.2
Shortcut Models Frans et al. [2025]	64	400K	20.5
MeanFlow Geng et al. [2025a]	64	400K	12.4
Long-Short Flow Map / Drifting (ours)			
Laplacian kernel ($B=64$, mixed lr)	64	400K	19.36
Laplacian kernel ($B=64$)	64	100K	28.12
Laplacian kernel ($B=256$)	256	100K	18.87
Laplacian kernel ($B=1024$)	1024	100K	14.71
Gaussian kernel ($B=64$)	256	100K	24.70
Gaussian kernel ($B=256$)	1024	100K	16.56



Figure 7: **Ablation study on feature-space optimization.** We compare three settings: using the default feature set with thousands of features (top), using only four features (middle), and operating directly in the original space (bottom).

ingly transforms the $\frac{\mathbb{E}_{x_1 \sim p_1(x_1|y)}[(x_1 - \psi_{0 \rightarrow 1}^\theta(x_0))k_1(x_1, \psi_{0 \rightarrow 1}^\theta(x_0))]}{\mathbb{E}_{x_1 \sim p_1(x_1|y)}[k_1(x_1, \psi_{0 \rightarrow 1}^\theta(x_0))]}$ term in Equation 13 and Equation 17 into $\frac{\mathbb{E}_{x_1 \sim p_1^w(x|y)p_1^{1-w}(x|\emptyset)}[(x_1 - \psi_{0 \rightarrow 1}^\theta(x_0))k_1(x_1, \psi_{0 \rightarrow 1}^\theta(x_0))]}{\mathbb{E}_{x_1 \sim p_1^w(x|y)p_1^{1-w}(x|\emptyset)}[k_1(x_1, \psi_{0 \rightarrow 1}^\theta(x_0))]}$.

3. **Other possible directions.** The above two options primarily modify the attraction component. Similar to Deng et al. [2026], one may also consider applying guidance to the impulse term

$\frac{\mathbb{E}_{x_1^\theta = \psi_{0 \rightarrow 1}^\theta(x'_0), x'_0 \sim p_0}[(\psi_{0 \rightarrow 1}^\theta(x_0) - x_1^\theta)k_1(\psi_{0 \rightarrow 1}^\theta(x_0), x_1^\theta)]}{\mathbb{E}_{x_1^\theta = \psi_{0 \rightarrow 1}^\theta(x'_0), x'_0 \sim p_0}[k_1(\psi_{0 \rightarrow 1}^\theta(x_0), x_1^\theta)]}$ in Equation 17.